SPECTROSCOPIC INVESTIGATIONS ON DNA AND BSA BINDING ABILITY OF A NEW PLATINUM (II) COMPLEX CONTAINING 5,6-DI(PYRIDIN-2-YL)-2,3-DIHYDROPYRAZINE LIGAND

A MASTER'S THESIS

in

Chemical Engineering and Applied Chemistry

Atilim University

by

ASMA MABROUK MOHAMED SALEM

July 2017

SPECTROSCOPIC INVESTIGATIONS ON DNA AND BSA BINDING ABILITY OF A NEW PLATINUM (II) COMPLEX CONTAINING 5,6-DI(PYRIDIN-2-YL)-2,3-DIHYDROPYRAZINE LIGAND

A THESIS SUBMITTED TO

THE GRADUATE SCHOOL OF NATURAL AND APPLIED SCIENCES

OF

ATILIM UNIVERSITY

BY

ASMA MABROUK MOHAMED SALEM

IN PARTIAL FULFILLMENT OF THE REQUIREMENTS FOR THE DEGREE OF MASTER OF SCIENCE

IN

APPLIED CHEMISTRY

AT

THE DEPARTMENT OF CHEMCAL ENGINEERING AND APPLIED CHEMISTRY

July 2017

Approval of the Graduate School of Natural and Applied Sciences, Atılım University.

_____

Prof. Dr. Ali Kara

I certify that this thesis satisfies all the requirements as a thesis for the degree of Master of Science.

_____

Prof. Dr. Atilla Cihaner

Head of Department

This is to certify that we have read the thesis "Spectroscopic investigations on DNA and BSA binding ability of a new platinum(II) complex containing 5,6-di(pyridin-2-yl)-2,3-dihydropyrazine ligand" submitted by "ASMA MABROUK MOHAMED SALEM " and that in our opinion it is fully adequate, in scope and quality, as a thesis for the degree of Master of Science.

_____	_____
Assoc. Dr. Filiz Korkmaz Özkan	Prof. Dr. Şeniz Özalp Yaman
Co- Supervisor	Supervisor

Examining Committee Members

Prof. Dr. Nezire Saygılı	_____
Prof. Dr. Şeniz Özalp Yaman	_____
Assoc. Prof. Dr. Alpan Bek	_____
Assoc. Dr.Belgin S. İşgör	_____
Assoc. Dr. Filiz Korkmaz Özkan	_____

Date: 14.07.2017

Statement of No Plagiarism

I declare and guarantee that all data, knowledge and information in this document has been obtained, processed and presented in accordance with academic rules and ethical conduct. Based on these rules and conduct, I have fully cited and referenced all material and results that are not original to this work.

Name, Last name: ASMA, SALEM

Signature:

ABSTRACT

SPECTROSCOPIC INVESTIGATIONS ON DNA AND BSA BINDING ABILITY OF A NEW PLATINUM (II) COMPLEX CONTAINING 5,6-DI(PYRIDIN-2-YL)-2,3-DIHYDROPYRAZINE LIGAND

ASMA MABROUK MOHAMED SALEM

Supervisor: Prof. Dr. Şeniz ÖZALP YAMAN

Co-Supervisor: Assoc. Prof. Dr. Filiz KORKMAZ ÖZKAN

2017, 60 pages

Designing and synthesis of more effective and less toxic platinum complexes are one of the main aims of the researchers to overcome the side effects of the cisplatinum chemotherapy. For this purpose, a new platinum(II) complex containing 2,3-bis(2-pyridyl)-5,6-dihydropyrazine ($PtLCl_2$) was modelled to mimic the cisplatinum structure , then synthesized and identified by several spectroscopic techniques to assess its DNA and BSA binding ability in this work.

In order to elucidate the type of association of the complex to calf thymus DNA, UV titration, fluorometric titration, thermal decomposition and viscometry experiments were conducted under physiological conditions. Thermodynamic parameters were also determined from the UV titrations which are iterated at different temperatures. It is found that $PtLCl_2$ interacts with DNA through groove binding or electrostatically.

Binding ability of $PtLCl_2$ to BSA (Bovine Serum Albumin) was also tested with the similar techniques that were used formerly in the DNA association studies. The results clearly indicated that the complex interacted with the hydrophobic region of the protein electrostatically leading an increase in hydrophilicity of the protein.

The IR analysis made specifically for identifying the binding side of the complex to BSA were also confirmed increasing in the hydrophilicity of the protein with the effect of $PtLCl_2$.

Keywords: Antitumor drugs, platinum complexes, -nitrogen donor ligands, DNA binding ability, BSA binding ability.

ÖZ

5,6-DI(PYRIDIN-2-YL)-2,3-DIHYDROPYRAZINE LİGAND İÇEREN YENİ PLATİN(II) KOMPLEKSİNİN DNA VE BSA'YA BAĞLANMA BAĞLANMA KABİLİYETİNİN SPEKTROSKOPİK OLARAK İNCELENMESİ

ASMA MABROUK MOHAMED SALEM

Supervisor: Prof. Dr. Şeniz ÖZALP YAMAN

Co-Supervisor: Assoc. Prof. Dr. Filiz KORKMAZ ÖZKAN

2017, 60 pages

Cisplatin kemoterapi tedavisinin yan etkilerinin azaltılması için daha etkin ve daha düşük toksisite değerlerine sahip yeni platin kompleksleri tasarlayarak sentezlerini gerçekleştirmek bu alanda çalışan araştırmacıların ana amacıdır. Bu gaye ile, çalışmamızda cisplatinin yapısal bir benzeri olarak 2,3-bis(2-pyridil)-5,6-dihidropyrazin içeren yeni bir platin kompleksi ($PtLCl_2$) modellenmiş, sentezlenmiş ve yapısal analizleri çeşitli spektroskopik yöntemler kullanılarak tamamlanmıştır.

Kompleksin DNA'ya bağlanma tipini belirleyebilmek için UV tirasyon, florometrik titrasyon, termal bozunma ve vizikometri deneyleri fizyolojik artamda yaılmıştır. Termodinamik parametreler yine UV titrasyon deneylerinin farklı sıcaklıklarda yinelenmesi ile elde edilmiştir. Deneyler sonucunda, $PtLCl_2$'nin DNA'nın boşluklarına tutunduğuya da elektrostatik bir etkileşim yaptığı bulunmuştur.

$PtLCl_2$'nin BSA ile etkileşimi DNA bağlanma deneylerinde kullanılan yöntemlerle benzer teknikler kullanılarak belirlenmiştir. Sonuçlar kompleksin BSA'ya proteinin hidrofobik bölgesinden bağlanarak hidrofilitesini artırdığını açıkça göstermiştir.

Ptotein- kompleks etkileşim alanının belirlenmesi için yapılan ayrıntılı FTIR spektroskopisi analizleri de $PtLCl_2$'nin etkisiyle proteinin hidrofilitesini arttığını doğrular sonuçlar vermiştir.

Anahtar Kelimeler: Antitumör ilaçlar, platin kompleksleri, kükürt azotverici ligandlar, DNA bağlanma kabiliyeti, BSA bağlanma kabiliyeti

ACKNOWLEDGMENTS

First and foremost, I am grateful to Allah almighty for giving me strength, knowledge, health and wisdom to undertake this work.

I would like to express my appreciation to my supervisor Prof. Dr. Şeniz Özalp Yaman for her support, guidance and patience during my study.

I would like to express my appreciation to my co-supervisor Assoc. Prof. Dr. Filiz Korkmaz Özkan for her support and help during my research.

I would like to express my thanks to Assis. Prof. Dr. Hüseyin Karaca from Sakarya University for their sincere support and help.

I am grateful to my family and my friends for support, trust and encouragement.

Also, I wish to express my thanks to all staffs in the Department of Chemical Engineering and Applied Chemistry at Atilim University for their efforts and helps.

TABLE OF CONTENT

LIST OF TABLES

LIST OF FIGURES

LIST OF ABBREVIATIONS

FTIR	-	Fourier Transform Infrared
CT-DNA	-	Calf-Thymus DNA
DMF	-	Dimethylformamide
DNA	-	Deoxyribonucleic acid
NMR	-	Nuclear Magnetic Resonance
UV–vis	-	Ultraviolet–visible Spectroscopy
ΔG^{o}	-	Standard Gibbs Free Energy
ΔH^{o}	-	Standard Enthalpy Change
ΔS^{o}	-	Standard Entropy Change

CHAPTER 1

INTRODUCTION

1.1 Cancer & Cures

As one of the diseases that perplexed the physicians, the scientists and the drugs developers over the years, cancer also is one of the most fatal illnesses in the human history. As per the latest statistics provided by the American Cancer Society in 2016, more than 1.68 million new cases are estimated this year along with 595,690 death cases with the cancer as the direct cause making it on the top of the death causes list with heart diseases [1]. However, the survival rate in the United States of the cases have increased from 49% in 1975 to 69% in 2011 which is mainly attributed to the advancement in the treatments and technologies used in fighting the different types of cancer at its several stages.

As some cells in the body are going through divisions and multiplications for a certain time period, cancer is developed by cells with damaged DNA and damaged DNA-repair mechanisms in certain body tissues [2]. Moreover, it is important to study the cell cycle in order to be able to understand the treatment mechanism which will be described in conjunction with the cell cycle illustrated in Figure 1.1 below [3].

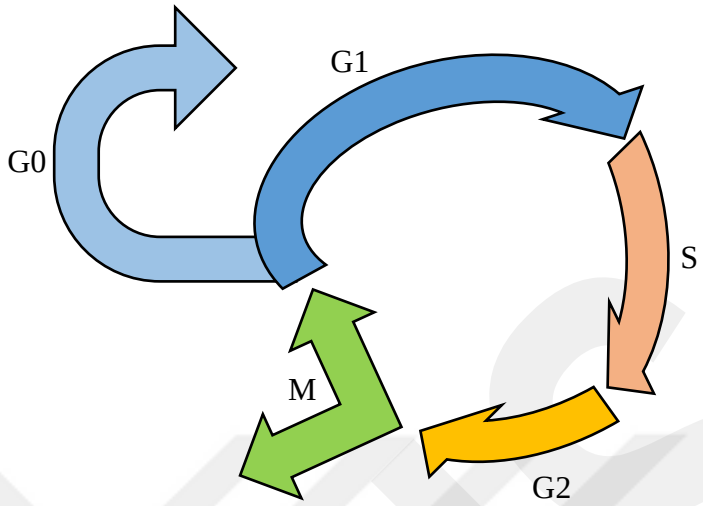

Figure 1.1. Phases of cell cycle.

G0 Phase (0 - few years): This is the status of most of the body cells where it is at a resting stage. When a body cell receives a signal to reproduce, it moves to the G1 Phase.

G1 Phase (18 – 30 hours): The cell cycle starts at this stage where the cell grows its protein and size.

S Phase (18 – 20 hours): DNA chromosomes start to get copied in order to fit in the new cells.

G2 Phase (2 – 10 hours): DNA checked and preparation for splitting.

M Phase (30 – 60 minutes): Also called Mitosis, splitting to two new cells that may go to the G0 phase or again to the G1 phase for further reproduction.

Furthermore, there are many treatment methods or strategies that are followed to cure cancer which includes surgery and radiotherapy. However, due to the systematic nature of the disease, another systematic treatment needed to be developed in order to increase the range of tumor types and stages that can be treated which came to reality with the development of chemotherapy drugs [4]. There are many groups of the chemotherapy drugs that are classified according to the way they deal with the cancer

cells and the cell multiplication process, explained in Figure 1.1 above as the chemotherapy drugs attack cells in the S and M phases, which the main types can be summarized as the following [3]:

1. Alkylating Agents: these drugs attack the reproducing cells at all phases. However, depending on dosage and treatment length these agents can damage the bone marrow and increase the risk of Leukemia.
2. Platinum Drugs: these drugs work in a similar way as the Alkylating Agents and sometimes are classified with them. Nonetheless, these drugs have less risks of causing Leukemia to the patient which make them more popular. This group include cisplatin which is part of the study of this thesis.
3. Antimetabolites: these drugs damage the cancer cells during the S phase during the chromosomes copying process.
4. Anti-Tumor Antibiotics: these drugs work on changing the DNA in the cancer cells in order to stop them from reproducing.
5. Topoisomerase Inhibitors: this type of drugs work with the enzymes which carry the same name in order to facilitate the DNA copying process during the S phase.
6. Mitotic Inhibitors: these drugs stop the M phase of the cell reproduction cycle.

In this thesis, the study will be performed on DNA and BSA binding with new Platinum II complexes (i.e. cisplatin) containing 5,6-di-(pyridine-2-yl)-2,3-dihydropyrazine Ligand. Moreover, the study will first include theoretical part where the reactions between the Platinum II complexes and DNA are studied along with previewing previous results from documented experiments and studies. Furthermore, practical experiments will be conducted in order to confirm the results and study the possibility for further efficiency.

1.2 Platinum Anti-Cancer Complexes

Using metal ions for medical treatments is a cure that has been used since ancient time, some dated to 5000 years ago. Continuous researches and experiments

continued discovering the effectiveness of such compounds due to their strong bonding to body agents such as proteins and enzymes [5]. The discovery path of the Platinum anti-Cancer complexes started in 1962 when Professor Barnett Rosenberg from the Biophysics department at Michigan State University was conducting an experiment on the prokaryotic cells and the effect of the electromagnetic field on their multiplication process. After finishing the experiment, Professor Rosenberg noticed a cluster of cells that remained undivided which he discovered later is a result of a dissolution of the electrodes made out of platinum and their reaction with chloride and ammonium ions [6]. From that starting point the developments continued for many years, which can be summarized as the following [6]:

1. In 1969, the first anti-cancer screening results were published in a scientific journal where cis-dichlorodiammineplatinum II, cis-$[PtCl_2(NH_3)_2]$, and cis-tetrachlorodiammineplatinum IV, cis-$[PtCl_4(NH_3)_2]$ were identified as influential anti-tumor screening agents.
2. In 1971, although the complex showed some toxic effects especially on the kidney, cisplatin, as shown in figure 1.2, was selected for preclinical evaluation by the National Cancer Institute of America and Institute of Cancer Research in UK.

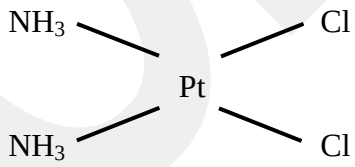

Figure 1.2. The first clinical used Cisplatin (NSC 119875).

3. Prior 1977, low dosages of cisplatin (20 – 30 mg/m^2 of body surface) in therapies as a single agent or combined with other agents which reduces the side effects on the kidney.
4. In 1977, a new technique was developed by giving mannitol-induced diuresis before or after giving the cisplatin which reduced the effects on the kidney and allowed the dose to go up to 120 mg/m^2. This breakthrough opened the door to more efficient chemotherapy using cisplatin with long-term remissions achieved over 90%.

1.3 Study Aim and Scope

The aim of the study is to synthesize a new platinum complex, namely [dichloro(5,6-di(pyridine-2-yl)-2,3-dihydropyrazine)platinum(II)] (PtL) and to investigate its DNA and BSA binding ability spectroscopically. These spectroscopic investigations were carried out by examining the PtL with DNA as well as with BSA protein. The following spectroscopic methods were used for obtaining results;

1. UV Titration
2. Viscosity
3. Thermal Decomposition
4. Fluorometry
5. FTIR

1.4 Thesis Structure

The aim of this thesis is to provide a sufficient theoretical background, display the results of the experiments, and discuss the results in order to provide a complete picture about the issue in question. Therefore, the structure of this thesis will be as the following:

Chapter One: A general introduction to the subject in addition to information about the different chemotherapy agents used in cancer treatment. Moreover, the chapter provides a brief history about the development of cisplatin complexes and specifies the aim and scope of the study. This chapter also includes a theoretical study of the cisplatin complex as part of the Platinum II complexes for anti-cancer functions. The study will preview previous results of experiments conducted on cisplatin and layout the methodology of the study experiments.

Chapter Two: An experimental approach to investigate the DNA and FTIR BSA binding with new Platinum II complexes (i.e. cisplatin) containing 5, 6 di(pyridine-2-yl)-2,3-dihydropyrazine Ligand through 4 tests; UV-interaction, viscosity, thermal decomposition and fluorometry.

Chapter Three: A discussion of the experiment results along with comparisons to previous experiments results for validation and improvement measurement. Furthermore, set of conclusions based on the theoretical and experimental parts of the study are provided. Moreover, further recommendations will be provided for future research projects.

1.5 Theoretical Review

This section will review the structure of anti-tumor complexes, with an emphasis on platinum complexes, the mechanism of interaction between the complexes and the DNA, and previous experiments within the same context of this research.

1.5.1 The DNA and Anti-Tumor Complexes' Mechanism

Metal complexes are the leading treatment for cancer cells by binding the DNA through several reactions, as well as cleaving duplex agents through several types of chemical reactions. There three ways which the treatment interacts with the DNA [7]:

1. Controlling transcription factors: this is not a direct interaction between the treatment and the DNA. However, the treatment reacts to the binding protein of the DNA to affect its function.
2. Creating a hybrid: the treatment in this method binds to an RNA, which then binds to the DNA. This process hinders the transcription of the DNA molecules.
3. Treatment and DNA binding: the ligand molecules bind with the DNA double helix.

The methodology in designing treatments associated with DNA activities and functions take many essential steps into consideration. Once the DNA of a certain disease is studied, Basic sequences which are vital for the organism's survival are identified. Thereafter, the complex is created to interact with the identified sequences within the organism's DNA. Furthermore, a balance should be created within the complex to achieve the targeted interaction without getting blocked by other unwanted

interactions. Nonetheless, the extent of applying the complex shall also be studied in order not to cause any impact of the human functions of the person. Moreover, the interaction between a complex and the DNA occurs through two main steps which are Binding and Cleavage [7].

1.5.1.1 Binding

This step describes the way the complex molecules interrelate to the DNA, which is divided mainly into three main types:

1. **Groove binding**

The molecules of the complexes that bind under this type react with either the major grooves at (G-C) pairs or minor grooves at (A-T) pairs of the DNA, the groove structure of the DNA is shown in Figure 1.3 below [8]. The molecules of the complex react with the DNA by fitting into the major or minor grooves. By replacing water in the grooves, the molecules, which are heterocyclic or aromatic hydrocarbon, rotate to fit into the grooves. Thereafter, the complex molecules search for the targeted DNA sequences. Once identified, the molecules bind with the DNA using a non-covalent bond, which allows it to react with the targeted sequence regardless of the groove type as shown in Figure 1.4 below [9].

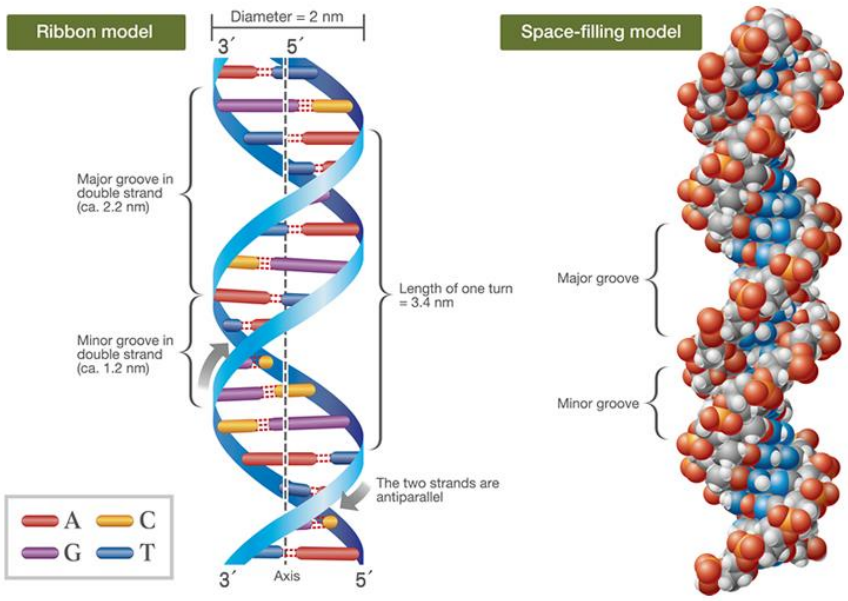

Figure 1.3. DNA groove structure [8].

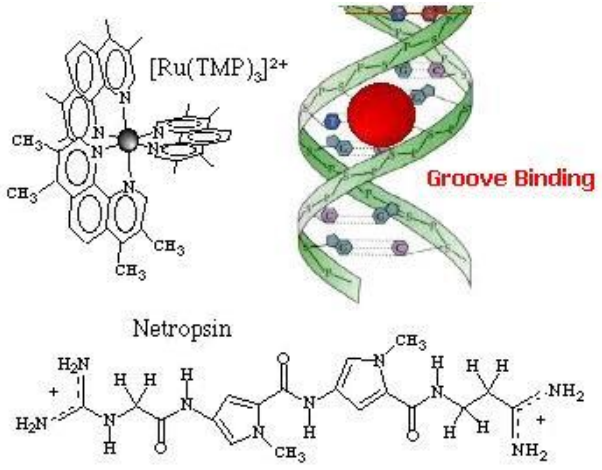

Figure 1.4. Binding of complex molecules with the groove structure [9].

Nonetheless, the complexes' molecules vary in their ability of binding with either the minor or major grooves as a certain type can bind with one type of groove. Therefore, a sequence of the rings of the heterocyclic or aromatic hydrocarbon binds with the DNA. As the DNA backbone gets closer together, this forms the minor grooves. On the contrary, as that distance get further, the major groove gets formed. Thereafter, this binding forms structures of two kinds, netropsin or distamycin, which the helix structure embraces their molecules allowing them to change the structure or control the transcription [10].

2. Intercalators

This methodology of binding gets executed through introducing a planar heterocyclic molecule within the DNA base pairs, which relaxes the DNA helical shape into a more enlengthened shape. Although they consist of aromatic or heteroaromatic molecules, these complexes can intercalate between the DNA pairs and achieve duplex stabilization without interfering to the pairing pattern. The mechanism of relaxing the helical shape and lengthening stops the DNA from replicating or performing and division operations. Furthermore, the result of this binding between the complex, the DNA and the topoisomerase kills the multiplying cells, which makes it to have more

influence on tumor cells rather than normal ones. Figure 1.5 below shows the complex result of intercalation with DNA [10].

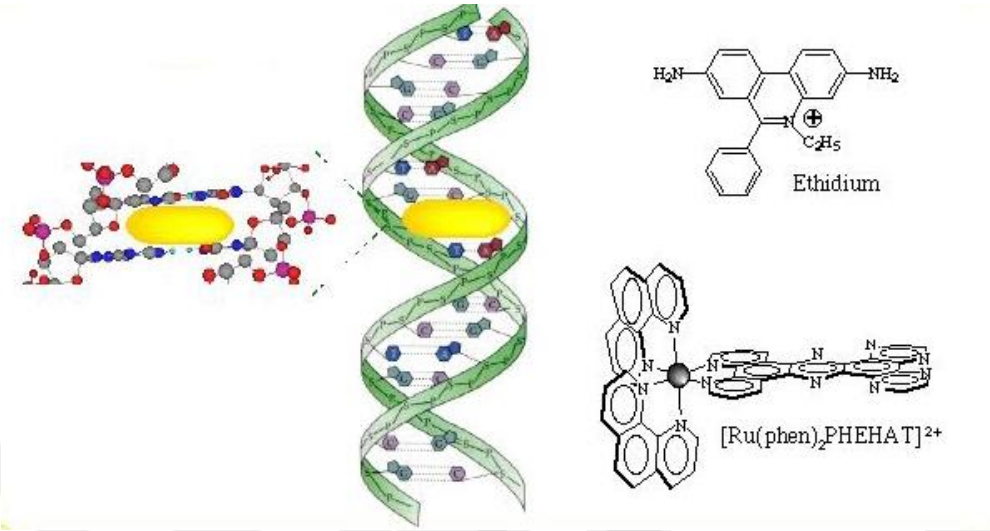

Figure 1.5. Intercalation of planar complex molecule in DNA [10].

3. Alkylators

These complexes contain strong electrophilic molecule, which cause a chemical reaction with the nucleophilic groups of the DNA forming a covalent bond, which is a process that occurs through a SN1 and SN2 reactions. Therefore, these complexes are mostly effective on the N (7) atom of Guanine and N (3) atom of Adenine, which are nucleophilic and uncovered in the helix structure. Nonetheless, there are many types of alkylators that target the DNA, specifically the Guanine part, or specifically the Adenine part of the DNA [9]. Cisplatin is part of this group and its structure and mechanism will be elaborated in section 1.5.2 of this research.

1.5.1.2 Cleavage

The DNA cleavage process is of splitting the strands of the DNA, which is essential to achieve apoptosis and then cell death. Anti-tumor complexes depend on this step to complete the desolation of the unwanted cells chemically, enzymically or using radiation. Therefore, the cleavage step is divided into three main types.

1. **Hydrolysis (Enzymatic)**

As the cell has the ability survive for billions of years in neutral mediums and ambient temperature, any complex needs to perform the hydrolysis in accelerated manner to reduce this timing to few minutes [7]. These reactions are performed through metal ions such as Lewis acids, which stimulate the phosphate part to form one of the following actions:

a. Nucleophilic attack
b. Activate water or hydroxide as nucleophile
c. Give the departing alcohol the ability to leave

Nonetheless, the mechanism which has an acceptable consensus on is the nucleophilic attack on the phosphate backbone of the DNA using the complex molecule, which facilitate forming a stabilized resultant from an intermediate compound. Thus, the cleavage occurs at the 3'-PO, as shown in figure 1.6 below, or 5'-PO, which cuts the strand and cause the cell to die [11].

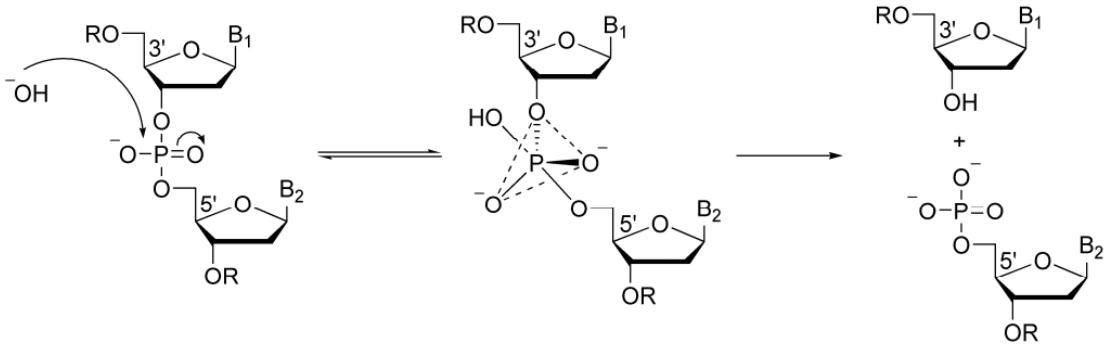

Figure 1.6. Hydrolysis cleavage of DNA [11].

2. **Photochemical (Using radiation to lead to chemical)**

This cleavage type is performed through either a UV-induced damage or producing reactive oxygen types, which establishes the relation in nature between the photochemical cleavage and the oxidative cleavage. In both methodologies, an oxygen type is the intermediate compound in the reaction, which is not the one causing the DNA damage. However, these initial intermediates result into other intermediate

compounds, which damage the DNA by putting it into auto-oxidation causing the strands to be cut [11]. Figure 1.7 below illustrate the photochemical cleavage equation.

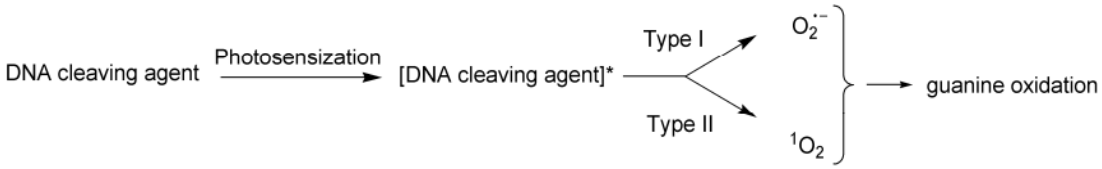

Figure 1.7. Photochemical cleavage equation [11].

In Figure 1.7 above, there are two main types for photochemical cleavage, which are one electron process (Type I), which is performed through exciting the cleavage agent to generate a superoxide radical through an electron transfer of an electron from an oxygen molecule leading to guanine oxidization, and pathway relating singlet oxygen (Type II), which is carried out through exciting the compound to generate a singlet oxygen modifying the guanine residues resulting into two pathways reaction as illustrated in Figure 1.8 below [7].

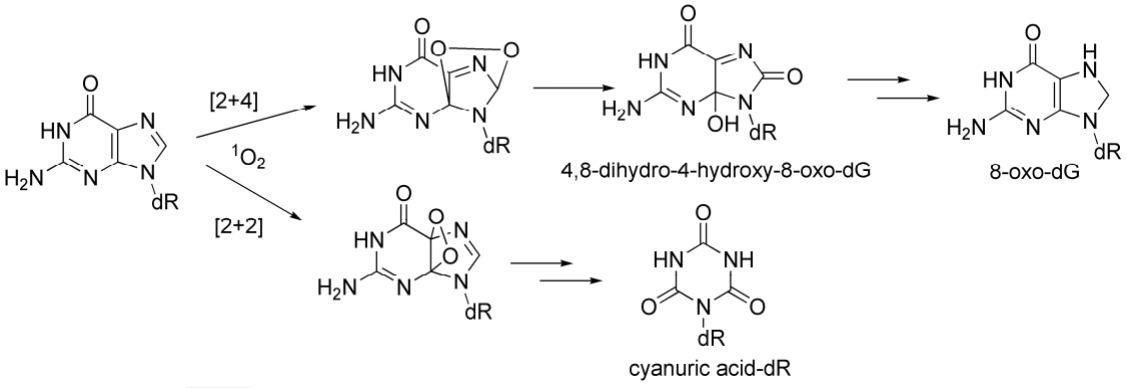

Figure 1.8. Guanine two pathway reactions in Type II Photochemical cleavage [11].

3. Oxidative (Chemical)

This type is performed by using agents that perform the second step of the photochemical cleavage, which its mechanism is explained above.

1.5.2 Cisplatin Mechanism

Cisplatin is an alkylator that reacts specifically with the Guanine N (7) atom, which forms a platinum-nitrogen bond that relaxes the helix structure, blocking transcription and killing the affected cell. Figure 1.9 below shows the mechanism of the Cisplatin in reaction with the DNA [7].

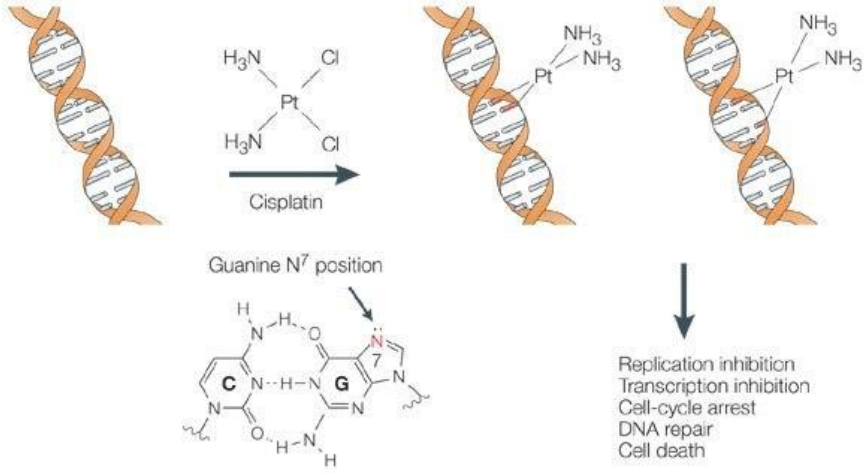

Figure 1.9. Cisplatin Mechanism with DNA [7].

1.5.3 BSA and Cisplatin Interaction and Mechanism

Bovine serum albumin (BSA) is a protein that is known to be the most abundant with up to 40 mg/ ml, and also the most present protein in plasma forming around 60% of the total protein in it. Therefore, understanding the interaction between BSA and any drug is essential in any pharmaceutical research due to its influence on the interaction

and absorption of the drug by the body. Moreover, BSA and human serum albumin are around 76% similar, which makes its results reliable [12].

In the history of related research, the chemical sequence of BSA and its crystal structure were discovered in the past few years. Furthermore, various compounds form a complex with serum albumins once introduced into the blood, which contributes to the osmotic pressure and keeping the pH at a balanced level in the blood. However, most of the albumins' interactions with several compounds are reversible [12].

On the interaction between BSA and metal complexes, examining fluorescence is one of the most important ways to assess it, through its intensive emissions when excited. The responsible parts of the fluorescence of the BSA is its structure which contains three amino acid residues that are natural fluorophore; tryptophan, tyrosine and phenylalanine, which has 100, 9 and 0.5 ratios, respectively. The methodology to examine fluorescence of the BSA is through the absence and presence of the cisplatin complex, where the blue and red changes in the maximum emission indicate the increase of the hydrophobicity [12].

BSA has a molecular weight of 66 kDa and has several functions in the human body including maintaining the normal osmotic pressure, binding to several substances and compounds, inactivating some compounds and an acid-base function. Moreover, BSA has discrete binding sites including site-I suited at hydrophobic cavity of subdomain IIA and site-II suited at hydrophobic cavity of subdomain IIIA. In researches, BSA is used to examine the interaction with ligands. The markers associated with the different sites are as the following [13]:

1. Site-I: includes warfarin, phenylbutazone, dansylamide, and iodipamide
2. Site-II: includes ibuprofen, flufenamic acid, and diazepam

In binding studies, examining BSA is significant due to the need to understand the drug pharmacodynamics and pharmacokinetics, which is carried out through evaluating the strength of the interaction in terms of absorption, distribution, metabolism and excretion. Moreover, the high similarity between BSA and Human Serum Albumin (HSA) makes the results reliable for drug testing [12] [13].

Studies suggest that BSA has a similar crystal structure to HSA, however, the detailed high resolution structure of BSA was recently discovered. In a study that compared the structure of BSA to HSA, it was mentioned that BSA has a heart-shaped molecule made out of three homologous α-helical domains (I, II and III), which each have subdomains called A and B subdomains [14]. Figure 1.10 shows on the the structure of BSA.

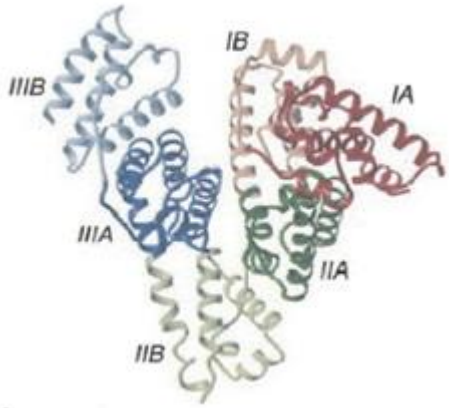

Figure 1.10. BSA structure [14]

BSA is composed of a lot of amino acids including tyrosine (Tyr) and Tryptophan (Trp), as effective interaction partners for drug delivery [15] [16]. These positively charged residues play an active role in carrying negatively charged ions, vitamins, hormones or any other substance that the protein shows affinity. The Structures of the aforementioned amino acids are shown in Figures 1.11 and 1.12.

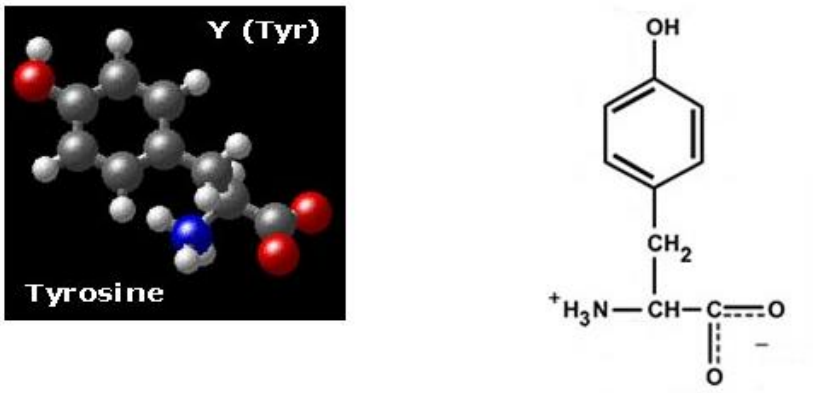

Figure 1.11. Tyrosine Structure [17]

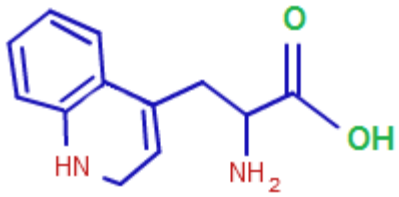

Figure 1.12. Tryptophan Structure [18]

1.5.4 FTIR

Infrared (IR) spectroscopy, which works through the vibrations of the molecules, examines the interaction between the electromagnetic radiation in infrared region with the molecules' electric dipole moment. It is a non-destructive method that provides immediate data on [19] [20]:

1. Bonds' order
2. Electrostatic interactions
3. H-bonding
4. Charge distribution
5. Protonation states
6. Redox states

7. Dynamics
8. Kinetics

The radiation is absorbed and the gained energy excites the molecules if the emitted radiation frequency is the same as the oscillation frequency of the molecule's vibration. Therefore, there are mainly three regions, which can be studied by IR spectroscopy, which ranges between 0.7 to 500 μm (20 to 1400 cm^{-1}) divided into three main ranges:

1. Near-IR: 0.8 to 2.5 μm or 4000 to 12500 cm^{-1}
2. Mid-IR: 2.5 to 25 μm or 400 to 4000 cm^{-1}
3. Far-IR: 25 to 100 μm or 10 to 400 cm^{-1}

An infrared spectrum is the plot of radiation absorption as a function of wavenumber ($\bar{\upsilon}$v), frequency (υ) or wavelength (λ), where r = c / λ and υ = 1 / λ; where c is the speed of light). The phenomenon of molecular vibration excitement of any sample provides unique absorption bands very closely in position in every biological material that have the same groups of structures, which creates a frequency for each group. Thus, absorption spectra of the compounds are known by their functional group frequencies of their molecules, which are interactive with the surrounding conditions. Moreover, those frequencies are also due to the motion of the nuclei, such as; twisting, bending, rocking and stretching modes (asymmetric and symmetric). Some of the vibrational modes of a triatomic molecule are illustrated in figure 1.13 below. Frequency values belonging to a specific mode of vibration are presented as (v_s) for symmetric stretching, as (v_{as}) for antisymmetric stretching, and as (δ) for bending modes.

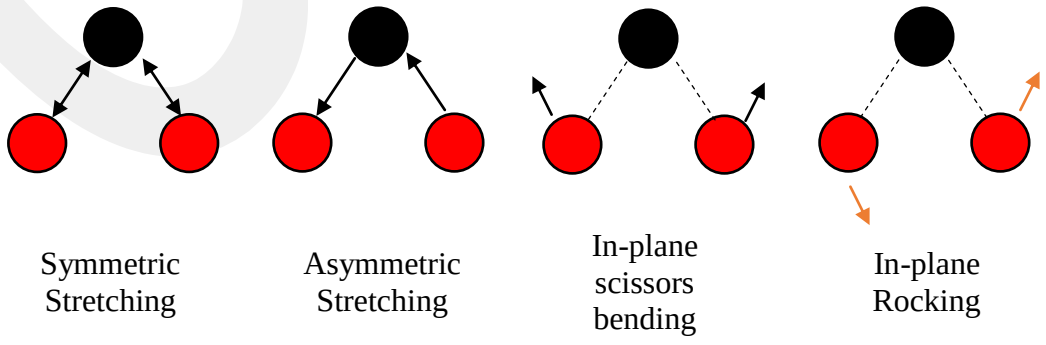

Figure 1.13. Vibrational modes of a triatomic molecule [20].

The vibration modes are divided into different categories. The main modes are the stretching and bending modes, and the latter includes four types, which are, in addition to the two modes on the right side of Figure 1.13, there are out-of-plane wagging and twisting modes.

CHAPTER 2

EXPERIMENTAL SECTION

2.1 Preparation of Compounds

2.1.1 5,6-di-(pyridine-2-yl)-2,3-dihydropyrazine (L)

The ligand (L) is prepared using the methods practiced in the literature [21] published by one of our colloborators, Dr. Hüseyin Karaca's research group, in Sakarya University and the ligand structure was identified by ^{1}H-NMR spectrum (Fig.2.1).

^{1}H NMR (400 MHz, $CDCl_3$, δ, ppm): 8.1 (d-H6, 2-pyridine) 7.80 ppm (d-H3, 2-pyridine), 7.62 (dd-H4, 2-pyridine), 7.03 ppm (dd-H5, 2-pyridine), 3.76 ppm (d- 4H, (NCH_2CH_2N)).

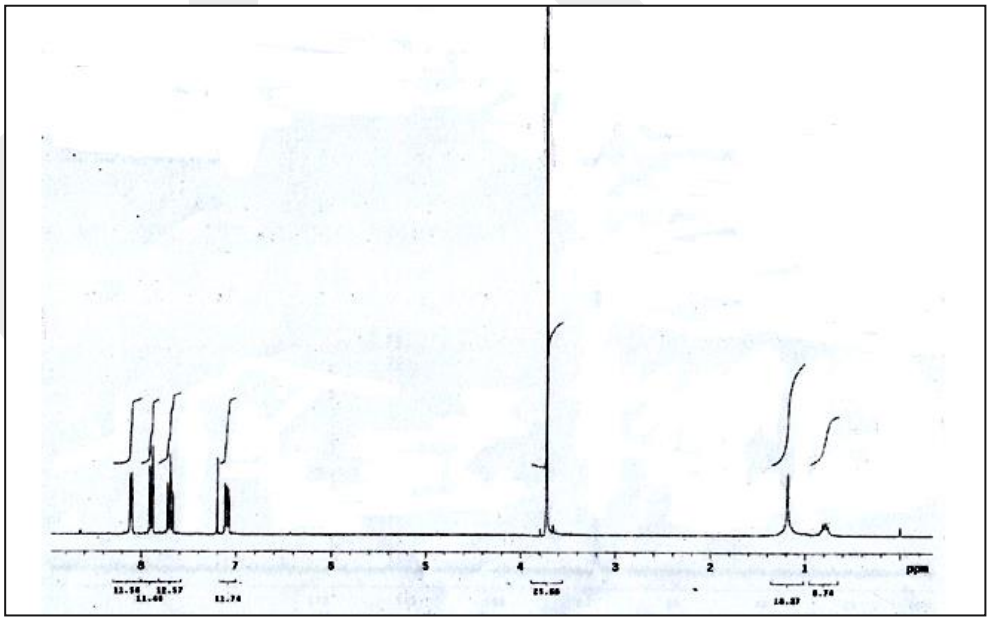

Figure 2.1. NMR spectrum of 5,6-di-(pyridine-2-yl)-2,3-dihydropyrazine (L) in $CDCl_3$.

2.1.2 [Dichloro(5,6-di(pyridine-2-yl)-2,3-dihydropyrazine)platinum(II)]mono hydrate, [($PtLCl_2$).H_2O]

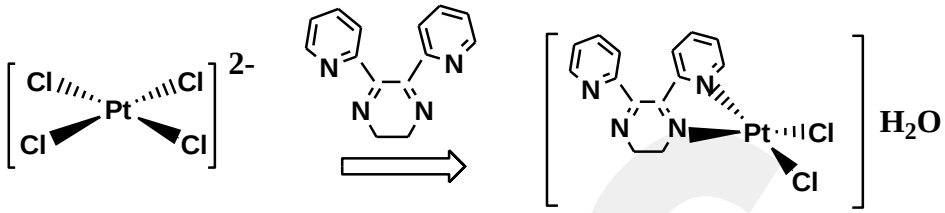

Figure 2.2. Preparation of the complex.

0.056923 g (0.241mmol) L, 5,6-di(pyridine-2-yl)-2,3-dihydropyrazine, was dissolved in 3 ml of DMF. On another side, 0.1 g (0.241mmol) of K_2PtCl_4 was dissolved in water. The platinum solution was added, on a drop basis, to the ligand-DMF solution and continuously stirred by a magnetic stirrer. Yellow-colored precipitate was observed and the resultant solution was refluxed at 40 ºC for 2 hours, which changed the precipitate color from yellow to dark brown. The solution was kept in the fridge overnight. Then, the dark brown precipitate of $PtLCl_2$ was collected under vacuum (Fig.2.2) and dried at room temperature. (%Yield: 27.52)

$PtLCl_2$ dissolves perfectly in DMF, however, it has less solubility in methanol, ethanol and acetone. H-NMR of the complex given in Figure 2.3 below.

Elemental Analysis: $PtC_{14}H_{14}N_4Cl_2O$: C, 32,32; H, 2.71; N, 10.77. Found: C, 32,07; H, 2.55; N, 11.26; ICP: Pt% 38.084, Found: Pt %, 37.8; ^{1}H NMR (400 MHz, d-DMSO (Fig 2.3.), ^{1}H NMR (400 MHz, d-DMSO, δ, ppm): 9.69 (d-H6, 2-pyridine) 9.05 ppm (d-H3, 2-pyridine), 8.69 (dd-H4, 2-pyridine), 7.97 ppm (dd-H5, 2-pyridine), 3.23 ppm (d-2H, (NCH_2CH_2N)), 3.41 ppm (d- 2H, (NCH_2CH_2N)) ; MS(EI) m/z= 520,3 [M+H_2O]; HRMS (EI) calcd: 520,284, found: 520,1381.

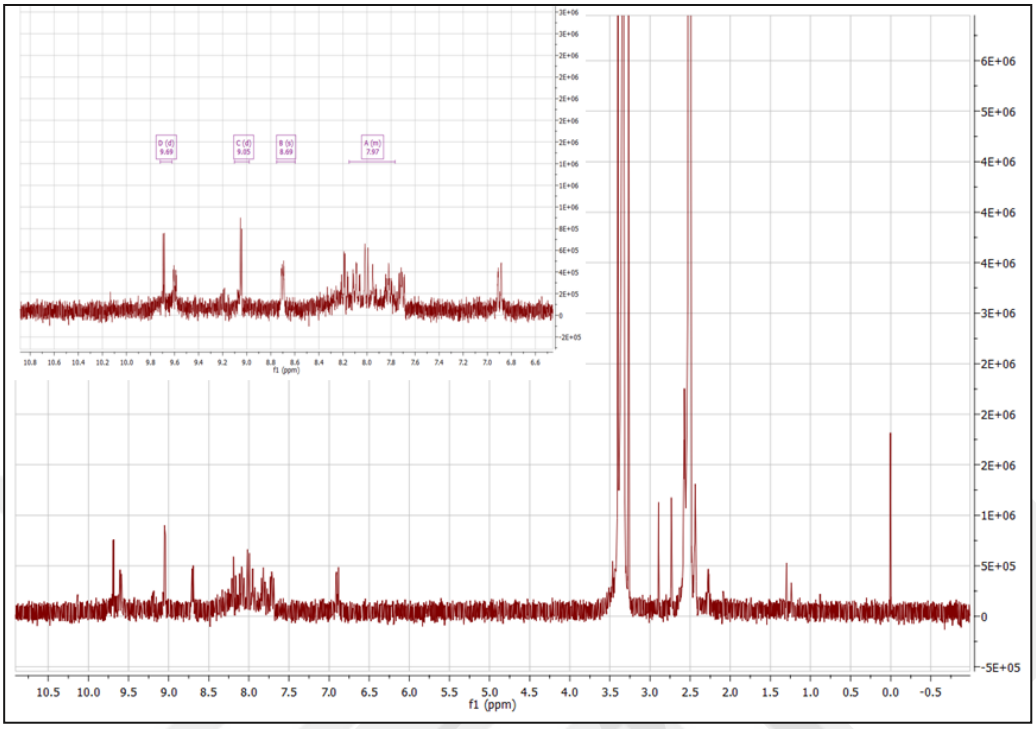

Figure 2.3. ^{1}H-NMR spectrum of [dichloro(5,6-di(pyridine-2-yl)-2,3-dihydropyrazine) platinum(II)] mono-hydrate, [($PtLCl_2$).H_2O].

2.2 DNA Binding Studies

2.2.1 Spectroscopic Titration

Using HP Agilent 8453 spectrophotometer, the electro-absorption spectra was tested at a constant concentration of $PtLCl_2$ complex of $1.92x10^{-3}$ M and an increasing concentration of Calf Thymus from zero to $2.2x10^{-4}$ M. The optimum incubation time for the interaction between the DNA and the $PtLCl_2$ complex was observed at 30 minutes at 37C. The intrinsic binding constant (K_b) of the $PtLCl_2$ complex is determined as 338 nm by using this equation [22][23];

$$\frac{[DNA]}{(\varepsilon_a - \varepsilon_f)} = \frac{[DNA]}{(\varepsilon_b - \varepsilon_f)} + \frac{K_b}{(\varepsilon_a - \varepsilon_f)} \qquad (1)$$

Where $\varepsilon_a = \frac{A_{abs}}{[Pt]}$ and ε_b is the extinction coefficient of bound and ε_f is the free complex. The experiments were performed to determine the binding constant (K_b) at different temperatures ranging from 310 to 340 K, at increments of 10.

2.2.2 Thermal Decomposition

In a buffer mixture of 5 mM of Tris HCl:50 mM NaCl, which forms a 1:1 (v/v) at a pH level of 7.4, a spectrophotometer (Agilent®8453) with an installed HAAKE temperature controlled circulator bath was used to measure the thermal decomposition. During the presence and absence of the platinum complex, measurements of the absorbance were taken at 260 nm, where the concentrations of the Calf Thymus DNA and the platinum complex were kept constant at 60 μM and increasing the temperature by 2°C every minute between 30°C and 90°C.

2.2.3 Viscosity

The viscosity is studied through the viscometer (AND® SV-10 VIBRO Viscometer) at the room temperature, while the $PtLCl_2$ concentration varied between 10 μM and 60 μM. The concentration of ct-DNA's is maintained at 50 μM in a 1:1 (v/v) buffer mixture of 5 mM of TRIS-HCl:50 mM NaCl at pH of 7.4. The viscosity measurements of the ct-DNA in the presence (η) and the absence (η_o) of the $PtLCl_2$ are made automatically by the viscometer. A plot of $(\eta/\eta_o)^{1/3}$ versus 1/R was obtained.

2.2.4 Fluorometry

Using a fluorescence spectrometer (Thermo-Scientific® Lumina), the fluorosence intensity was measured keeping the ethidium bromide and ct-DNA concentration constant and changing the $PtLCl_2$ concentration in a buffer mixture of 5 mM of TRIS HCl:50 mM NaCl, which forms a 1:1 (V/V) mixture at pH of 7.4. The fluorescence spectrum of ethidium bromide-ct-DNA adduct was measured at a

wavelength of 610 nm, with the emission wavelength of 478 nm by the machine's software. Using the Stern-Volmer equation below, the spectra were analyzed [24]:

$$\frac{I_o}{I} = 1 + K_{sv} \, . r \quad (2)$$

Where I_o represents the fluorescence intensity at 610 nm in the absence of the quencher with the concentration (r) and I represents the fluorescence intensity at the same wavelength in the presence of the quencher with the same concentration. Moreover, K_{sv} is the linear Stern-Volmer constant.

2.3 BSA Binding Studies

2.3.1 Spectroscopic Titration

Using HP Agilent 8453 spectrophotometer, the electro-absorption spectra was tested at a constant concentration of $PtLCl_2$ complex of $5.67x10^{-4}$ M an increasing concentration of BSA from zero to $2.2x10^{-4}$ M. The optimum incubation time for the interaction between the BSA and the $PtLCl_2$ complex was observed at 45 minutes at 37C. The intrinsic binding constant (K_b) of the $PtLCl_2$ complex is determined as 278nm in 0.5 M sodium phosphate buffer at pH 7.4.

2.3.2 Thermal Decomposition

By using phosphate buffer (NaPi) at pH 7.4, a spectrophotometer (Agilent®8453) with an installed HAAKE temperature controlled circulator bath was used to measure the thermal decomposition. During the presence and absence of the $PtLCl_2$ complex, measurements of the absorbance were taken from the peak at 280 nm, where the concentrations of the BSA was kept at 20.2 μM and $PtLCl_2$ at 2.245 μM, respectively, and increasing the temperature by 2°C every minute within the range of 60 to 120°C.

2.3.3 Viscosity

Viscometric measurements were performed by using AND® SV-10 VIBRO Viscometer at room temperature. The platinum complex concentration ranged between 5 μM and

25 μM while that of BSA has been kept constant at 25 μM in the sodium phosphate buffer. The viscometric data measurements were treated as a plot of $(\eta / \eta_o)^{1/3}$ versus 1/R , where η_o and η represent the viscosity data in the absence and the presence of the BSA, respectively.

2.3.4 Fluorometry

Using a fluorescence spectrometer (Thermo-Scientific® Lumina), the fluorometry was measured keeping the BSA's concentrations constant at 1 μM and the $PtLCl_2$ complex concentration was changed between 0 to 50 μM in 0.1 M phosphate buffer, at a pH level of 7.4 and 45 min. incubation time. The fluorescence spectra of ethidium bromide were measured at a wavelength of 280 nm, while the emission is at around 346 nm. The spectra were analyzed by using the Stern-Volmer equation as described for DNA binding experiments in section 2.2.4.

2.4 FTIR

2.4.1 FTIR Spectroscopy Measurements

BSA was dissolved in 0.1 M NaPi buffer at pH 7.4 to get a final concentration of 2.5 mM. An appropriate amount of powder $PtLCl_2$ was weighed and added to the BSA solution so that the final molar ratio of protein to compound was seven (R = 7). BSA blank and BSA and $PtLCl_2$ sample were incubated for 15 days using a heated circulating water bath at 37°C. The next day, another set of the same sample was prepared identically as the first set and started incubation. This way, there were two sets of samples (blank BSA and BSA - $PtLCl_2$) all incubated at physiological conditions, so that every experiment was performed at two times. Samples were measured hourly in the first six hours of incubation and afterwards measured daily at the same hour of the day during the 14 days' incubation period.

5 μl of the sample was dried on ATR unit to get rid of the excess water in the sample, therefore, provide better visualization of amide-I and II profiles of the sample. Infrared

(IR) absorbance spectrum was recorded with Nicolet 6700 (Thermo-Fisher Scientific Inc., USA) spectrometer equipped with DTGS detector. 64 scans were averaged for a final resolution of 4 cm^{-1}. The sample chamber inside the spectrometer was constantly purged with dry air. Empty chamber was used for background measurement, which then was automatically subtracted from the sample spectrum by the software OMNIC 3.2 (Thermo-Fisher Scientific Inc., USA).

CHAPTER 3

RESULTS AND DISCUSSIONS

3.1 Identification of the complex, $PtLCl_2$

3.1.1 Electronic Absorption Spectrum

The electronic absorption spectrum of $PtLCl_2$, which was captured in DMF and the extinction coefficient, ε, for each band, was shown in Table 3.1. The electronic absorption spectrum of the $PtLCl_2$, as seen in Figure 3.1 below, has an intense band at 279 nm, which is attributed to n→π* [25] and 340 nm is assigned as π→π* charge transfer transition involving the electron of the heterocyclic nitrogen atoms [26]. Moreover, the weak transitions 409 nm for $PtLCl_2$ complex may attributed to d^8-platinum(II) spin forbidden d-d-transitions [27].

Table 3.1: Electronic absorption spectral data for the $PtLCl_2$ complex in DMF.

Band No.	$\bar{\nu}$ (cm^{-1})	$\lambda_{(nm)}$	$\varepsilon_{(M^{-1}cm^{-1})}$
I	**35842.29**	**279**	**6905.457**
II	**29411.76**	**340**	**3014,547**
III	**2449.88**	**409**	**1483.776**

.

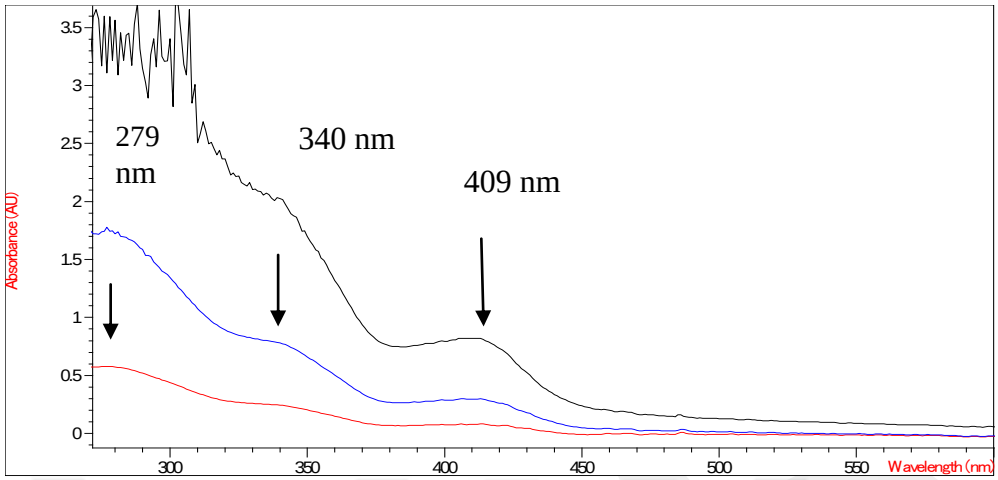

Figure 3.1. Electronic absorption spectrum of $PtLCl_2$ in DMF.

3.1.2. Infrared Spectrum

The peaks observed at around 1632 cm^{-1} is attributed to an aromatic $\nu_{(N-C)}$ stretching vibration [28] in pyridine ring (Table 3.2 and the Figures 3.2 A and B).

The peaks appeared at about 1566 and 1587 cm^{-1} are assigned to the aromatic N=C stretching frequencies of the ligand. The aromatic stretching of $\nu_{(C-H)}$ vibration, on the other hand is observed at about 3018 cm^{-1}. While aromatic ν(C=C) vibrations are obtained around 1345-1464 cm^{-1}, the aromatic ν_{C-C} starchings appeared in the region of 1476-1531 cm^{-1}.

In IR spectrum of the ligand, the peaks in the range of 745-895 cm^{-1} and 625-697 cm^{-1} are most probably due to the $\nu_{(C-H)}$ rocking and $\nu_{(C-H)}$ vibrations, respectively. The peak observed at 562 cm^{-1} is assumed to be $\nu_{(CCC)}$ as in plane deformation vibration [28].

In the IR spectrum of the $Pt(L)Cl_2$, the ν(O-H) vibration peak at 3384 cm^{-1} clearly indicates the monohydrate structure of $PtLCl_2$. Similarly, the deviation on the ν_{N-C} stretching (1652 cm^{-1}) and $\nu_{N=C}$ vibration (1568-1588 cm^{-1}) frequencies confirming the coordination (Table 3.2) of Pt ions to N-atoms of pyridine ring.

Table 3.2: Infrared vibration frequencies (cm^{-1}) for the ligand and the complex.

Peak Assignments	Vibration frequencies of L (cm^{-1})	Vibration frequencies of $Pt(L)Cl_2$ (cm^{-1})
ν(N-Pt-N)	-	479
ν(C=C) aromatic	1464 1447 1435 1345	1435 1403 1355
ν(C-C) streching aromatic in ring	1476 1531	1477 1524
ν(N=C) aromatic	1587 1566	1588 1568
ν(N-C) aromatic	1319 1281	1325 1291
ν(=C-H) bending	1149 1091 967	1164 1104 1067
ν(N-C) aromatic	1632	1652
ν(C-H) rocking	745 792 815 858 895	784 761 813 839 863
ν(C-H) aromatic stretching	3018	3063
ν(O-H)		3384
ν(C-H) bending	697 625	681 621 590
ν (CCC) in plane deformation	562	557

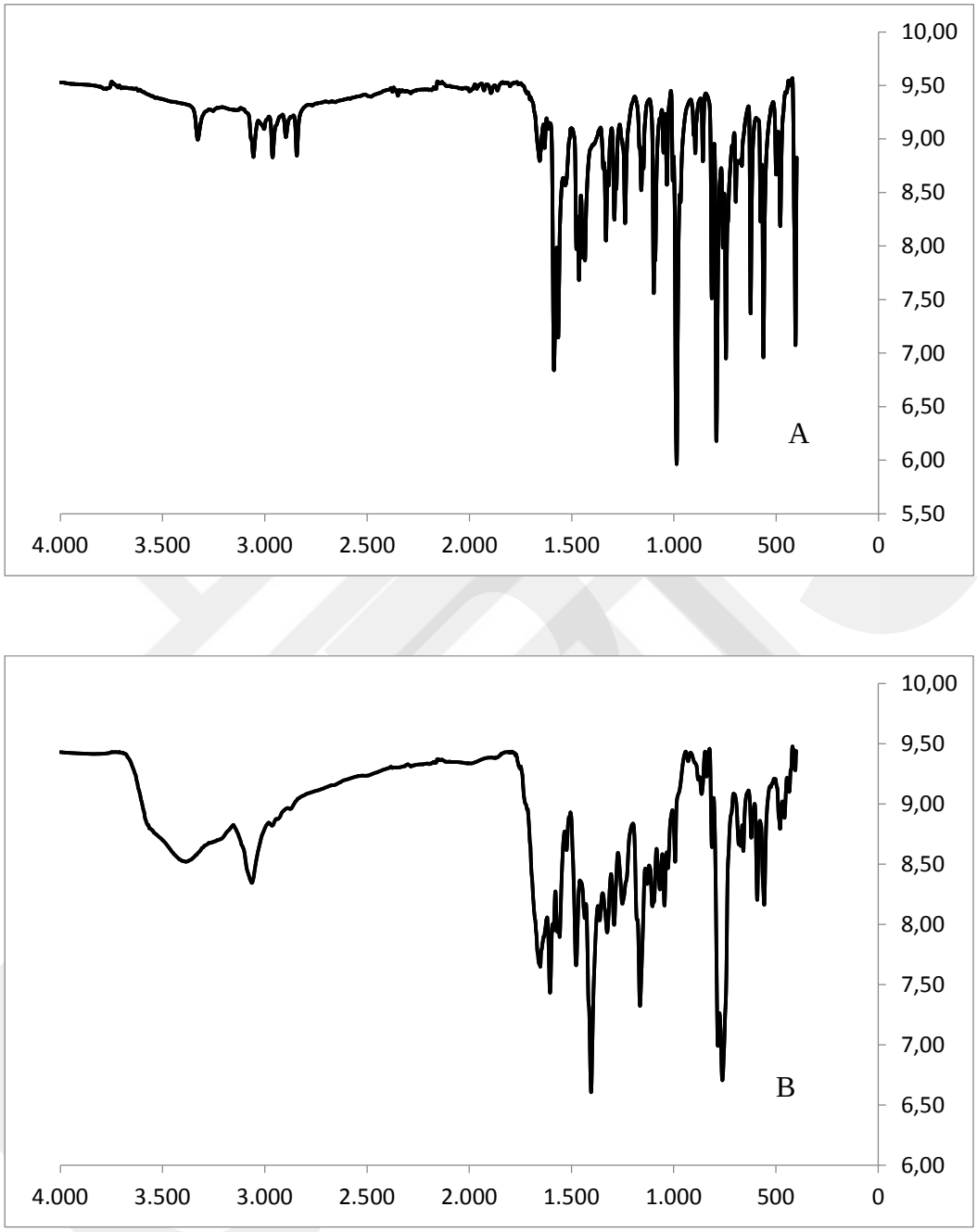

Figure 3.2. IR Spectrum of L (A) and $Pt(L)Cl_2$ (B).

The shift on the frequencies of aromatic C=C vibration of $PtLCl_2$ is about 10 cm^{-1}, which appears at 1355-1435 cm^{-1} by means of the coordination of the ligand. Likely, the deviation in the aromatic C-H stretching vibration frequency is about 40 cm^{-1} as depicted in Table 3.3. While the =C-H bending vibration frequencies are observed at about 1149-967 cm^{-1}, the peaks at around 745-895 cm^{-1} is attributed as C-H rocking. The C-H bending vibration of the coordinated ligand, however, is observed in the region of 625-697 cm^{-1}.

A new peak appeared in the IR spectrum of the complex at 479 cm^{-1}, assigned to N-Pt-N vibration [28].

As a conclusion, the observation of the N-Pt-N peak vibration frequency and the shifts in the characteristic vibration frequencies of the aromatic group indicates the formation of our pure $PtLCl_2$ complex.

3.1.3 ^{1}H-NMR Spectrum

Proton NMR of $Pt(L)Cl_2$ and L (2,3-bis(2pyridyl)-5,6-dihydropyrazine) were taken in d-DMSO and $CDCl_3$, respectively. Table 3.3 shows the chemical shifts of the complex.

Table 3.3 ^{1}H-NMR data for the ligand and the complexes

Compound	^{1}H-NMR
L ($CDCl_3$)	**8.1** (d-H6, 2-pyridine), **7.80** ppm (d-H3, 2-pyridine), **7.62** (dd-H4, 2-pyridine), **7.03** ppm (dd-H5, 2-pyridine), **3.76** ppm (d- 4H, (NCH_2CH_2N)).
$Pt(L)Cl_2$ (d-DMSO)	**9.69** (d-H6, 2-pyridine) **9.05** ppm (d-H3, 2-pyridine), **8.69** (dd-H4, 2-pyridine), **7.97** ppm (dd-H5, 2-pyridine), **3.23** ppm (d-2H, (NCH_2CH_2N)), **3.41** ppm (d- 2H, (NCH_2CH_2N))

The pyridine protons of L appear at around between δ 7.03 and 8.1 ppm, and that of the dihydropyrazine group exists at about 3.76 ppm (Table 3.3).

The ^{1}H-NMR spectrum of the platinum complexes consists of aromatics peak in the range of 7.97-9,69 ppm. The shift in the peak positions of the aromatic protons as well as the $–CH_2$ group of the pyrazine (3.23 and 3.41 ppm) to the lower region suggests the coordination of the ligand to the platinum(II) ion through its N-donor. However, the proton NMR of the platinum complex is not too clear to make good suggestions, because of the low concentration of the highly colored complex solution used in NMR.

3.2 DNA Interaction

3.2.1 UV-VIS

The DNA interaction with the platinum complex is seen via the spectral changes caused by the electronic absorption spectrum of ct- DNA. A broad band is shown at 260 nm in the UV area as illustrated in the UV-Vis absorption spectrum of DNA in Tris HCl buffer, which is caused by the electronic transition within the chromophoric groups in purine and pyrimidine base moieties. Few changes are also noticed in the absorption maximum and the molar absorptivity, which happened with the variations in pH or ionic strength of the medium. The study of DNA-drug interaction is examined by comparing the electronic absorption spectra of the standalone complex and the DNA-complex adduct, the intercalation binding with DNA is proven to result into hypochromism, bathochromism or hypsochromism, which are exhibited through decrease in the band intensity, a slight red shift, or slight blue shift, respectively. A stacking interaction between the base pairs of DNA and an aromatic group takes place, where the extent of the hypochromism is a proof of the strong intercalative interaction [29]. At the electrostatic attraction between the complex and the DNA, hyperchromic effect is illustrated. Hyperchromic effect, where in the band intensity increases, exhibits any conformational change on the DNA-helix after the DNA-complex interaction. The observed increase in the absorption is due to the denaturation of DNA double strand [29,30].

To examine if the 5,6-di(pyridine-2-yl)-2,3-dihydropyrazine coordinated platinum(II) complex interact with the DNA, an incubation process is executed as explained in the experimental section for the ct-DNA with the $PtLCl_2$, and its electronic absorption spectra were monitored in the presence and the absence of CT-DNA as shown in Figure 3.3.

When concentrations of ct-DNA solution were added to the constant concentration of the $PtLCl_2$ solution incrementally, an increase in the band intensities, caused by hyperchromism, was shown. The extent of the increase in the absorption of the LMCT (Ligand to Metal Change Transfer) band of the $PtLCl_2$ complex at around 338 nm was evaluated as 43.9%.

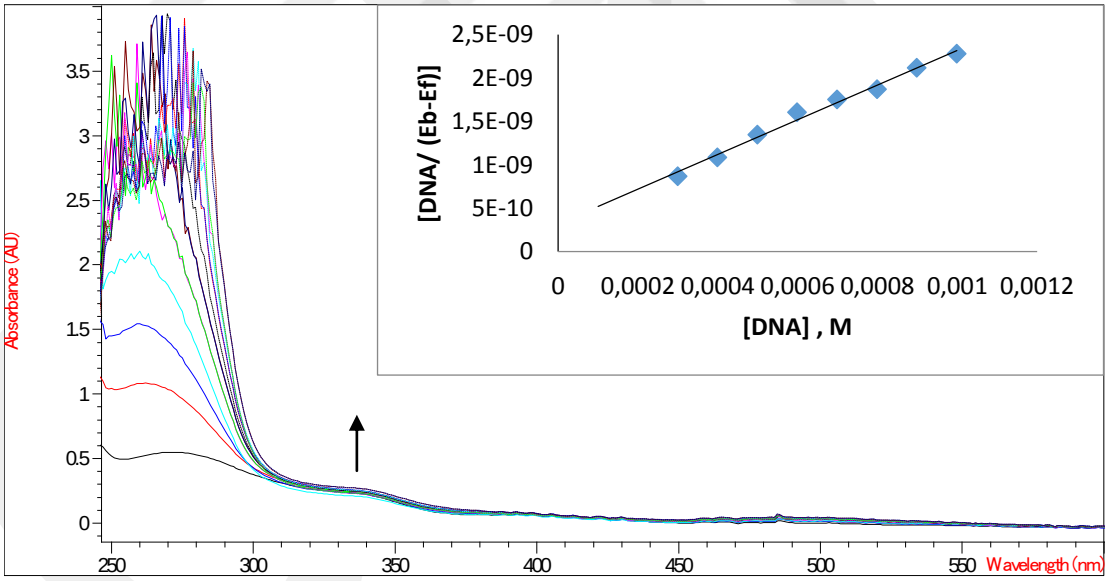

Figure 3.3. Electronic absorption spectra of the platinum complex in Tris-HCl buffer (pH = 7.2) in the absence and in the presence of increasing amounts of CT-DNA. Inset: Plot of $[DNA]/[\varepsilon_a - \varepsilon_f]$ *vs.* [DNA] at 37 ^{o}C.

The flowing equation was utilized to get the intrinsic binding constant of complex (K_b) with ct-DNA [38]:

$$\frac{[DNA]}{(\varepsilon_a - \varepsilon_f)} = \frac{[DNA]}{(\varepsilon_b - \varepsilon_f)} + \frac{K_b}{(\varepsilon_a - \varepsilon_f)}$$

Through the above equation, [DNA] is the concentration of DNA in base pairs, the apparent absorption coefficient, ε_a, ε_f, and ε_b correspond to $A_{obsd}/[Pt]$, the molar absorptivity constant for the free and the bound form, respectively.

K_b was obtained equal to $6{,}67x10^3$ M^{-1} from the ratio of slope to intercept by using the plots of [DNA]/$(\varepsilon_a - \varepsilon_f)$ versus [DNA]. This value is less than the K_b values reviewed in the literature or the classical intercalators such as ethidium bromide (K_b =$7x10^7$ M^{-1}) [31]. Nonetheless, the K_b value of the $PtLCl_2$ is at least five times higher than K_b values or same groove binder complexes [32,33]. Nevertheless, these results clearly suggest that the $PtLCl_2$ complex bind to DNA by electrostatic or groove binding mode.

In order to investigate the nature of interaction between the $PtLCl_2$ complex and the DNA, the temperature dependent binding constants (K'_b) were calculated at 47, 57 and 67 ^oC by iteration of the similar experiments (Fig. 3.4). and data is shown in Table 3.4. The standard Gibbs Free Energy change (ΔG^o) was calculated by using the equation below:

$$\Delta G^\circ = -R\,T\,Ln\,K'_b$$

In the above equation R and T represent the gas constant (8.314 J/mol.K) and the temperature (K), respectively. The standard binding enthalpy (ΔH^o) and the entropy (ΔS^o) of the $PtLCl_2$ was calculated by using the van't Hoff equation below (Fig. 3.5) [34]:

$$Ln(K'_b) = \frac{-\Delta H^\circ}{RT} + \frac{\Delta S^\circ}{R}$$

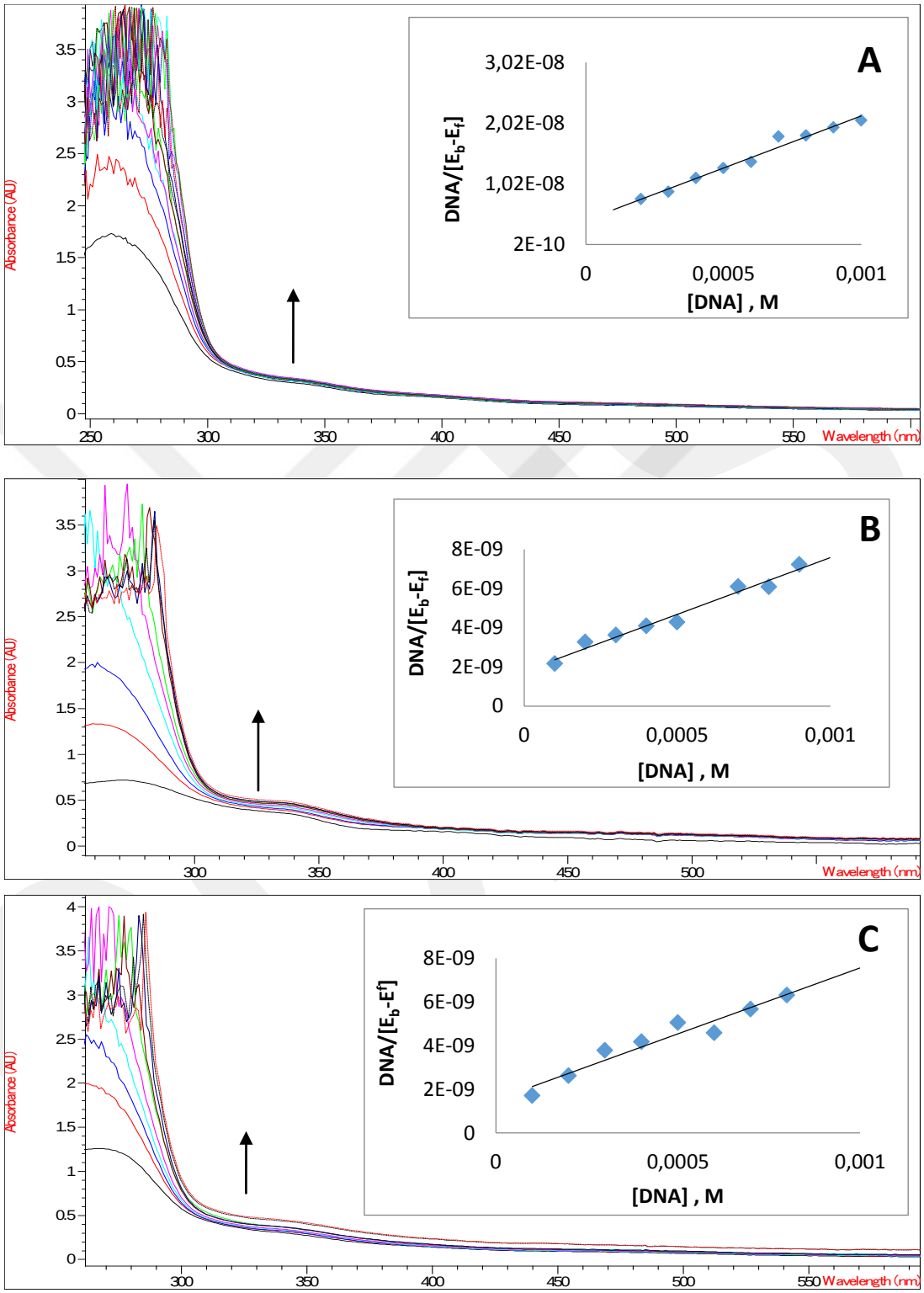

Figure 3.4. Electronic absorption spectra of the platinum complex at **(A)** 45 ^{o}C, (B) 57 ^{o}C and (C) 67 ^{o}C, respectively in Tris-HCl buffer (pH = 7.10) in the absence and in the presence of increasing amounts of CT-DNA. Inset: Plot of [DNA]/[$\varepsilon_a - \varepsilon_f$] *vs.* [DNA].

The intrinsic binding constant of complexes (K_b) with ct-DNA was obtained by using the following equation [30].

$$\frac{[DNA]}{(\varepsilon_a - \varepsilon_f)} = \frac{[DNA]}{(\varepsilon_b - \varepsilon_f)} + \frac{K_b}{(\varepsilon_a - \varepsilon_f)}$$

Generally negative enthalpy changes indicate that the binding is mainly enthalpy driven while the negative entropy indicates that the binding is unfavorable for it. In other words, van der Waals interactions and hydrogen bonding is suggested as a binding mode of the platinum complex by to DNA by confirming an electrostatic or groove binding the mode of action [35].

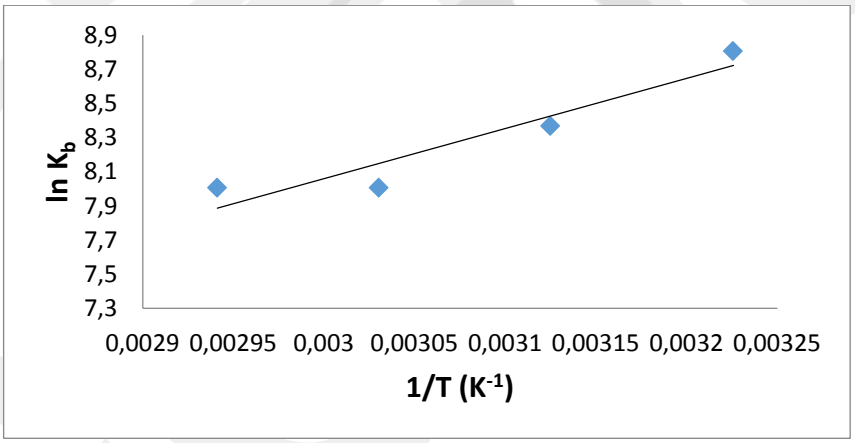

Figure 3.5. The linear Van't Hoff plot based on ln K_b versus 1/T.

Table 3.4: ΔG°, ΔH° and ΔS° data for DNA-$PtLCl_2$ adduct

TEMP(K)	K_b (M^{-1})	ΔG° (J)	ΔH° (kJ)	ΔS° (J/K)
310	$6.67x10^3$	-19356,271	-24.37	-6.094
320	$3.30x10^3$	-21181,703		
330	$3.00x10^3$	-22476,467		
340	$3.00x10^3$	-26516,548		

As clearly observed from the Table 3.4, the negative values of ΔG^o revealed the interaction process is spontaneous, while the negative values of ΔS^o indicate that the binding is mainly entropy driven and the enthalpy is favorable for it [36].

3.2.2 Thermal Decomposition

Thermal denaturation of CT-DNA is a method to determine the action mode of $PtLCl_2$ to DNA. While $PtLCl_2$ is present, information on the structural conformations and the strength of the DNA complex interaction are provided through the thermal behavior of DNA [37]. Interaction of metal drugs with the DNA helix may increase or decrease the melting temperature, T_m, of DNA. An increase in T_m value indicates an intercalative or phosphate binding while decrease is an evidence of base binding [38,39].

The thermal denaturation profile of the DNA and the $PtLCl_2$ -DNA adduct is presented in Figures 3.6 (A and B) below.

The T_m of ct-DNA was taken at 76℃ in the absence of $PtLCl_2$ (Figure 3.6A), while an increase of 1°C was observed in the T_m profile of the $PtLCl_2$ in comparison with the standalone DNA. As shown in the literature, the variance of the melting point of a few degrees Celsius proves an interaction involving groove binding and/or electrostatic binding to the phosphate group [40,41].

Therefore, it can be suggested that the pre-melting effect the $PtLCl_2$ complex is weak and the $PtLCl_2$ reacted with the phosphate groups electrostatically or performs groove binding through the double helix.

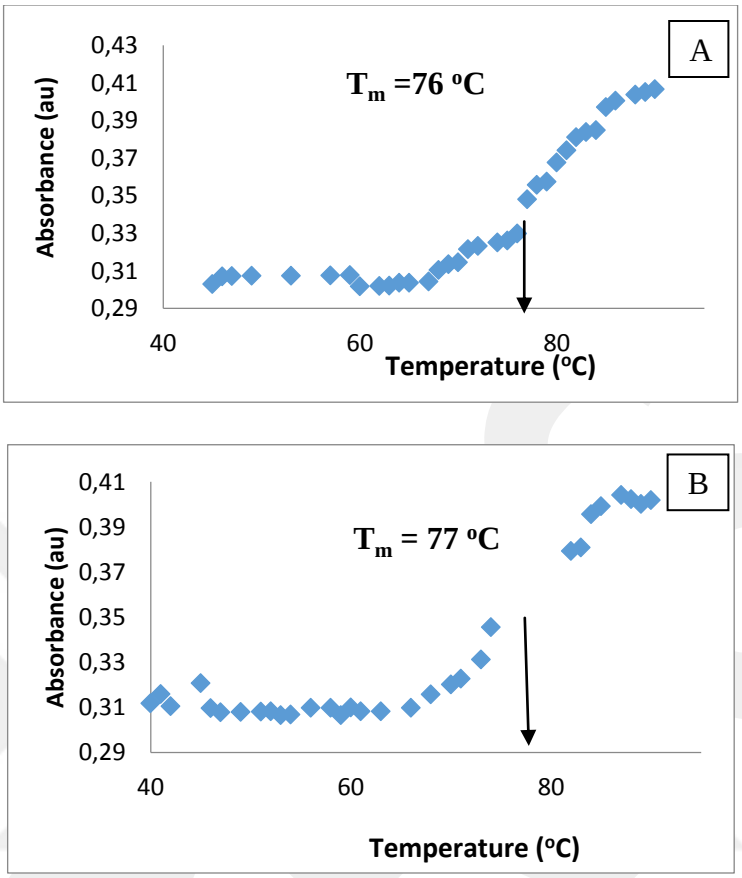

Figure 3.6. DNA and $PtLCl_2$ thermal decomposition (**A)** Without $PtLCl_2$ **(B)** With $PtLCl_2$.

3.2.3 Viscosity

Spectroscopic methods that were used provide important information about DNA-$PtLCl_2$ interaction but further support is needed to exhibit the binding model. Therefore, the viscosity examination is crucial to clarify the DNA-binding model, as the molecule length changes are shown through viscosity measurement. The intercalation process increases the length of the DNA strand caused by the separation of the base pairs, which is filled by the bound ligand causing the viscosity of the DNA to increase. The electrostatic interaction is a case where the compactness and aggregation on DNA occur, while the latter decreases the number of freely moving DNA molecules, which causes the decrease in viscosity of the DNA. Moreover, the viscosity is decreased by the

groove binding of complexes, which is caused by binding in the DNA helix and shortening the helical length [42].

The viscometric studies were carried out using SV-10 Vibro Viscometer in the presence and the absence of $PtLCl_2$ in the DNA-solution, which would indicate the binding mode of the complex. The viscosity variances of the ct-DNA in the presence $PtLCl_2$ are shown in Figure 3.7 below. The viscosity data are graphed as $(\eta/\eta_0)^{1/3}$ *vs* [$PtLCl_2$]/[DNA] concentration ratio, where η is the viscosity of the DNA in the presence and η_0 in the absence of the complex.

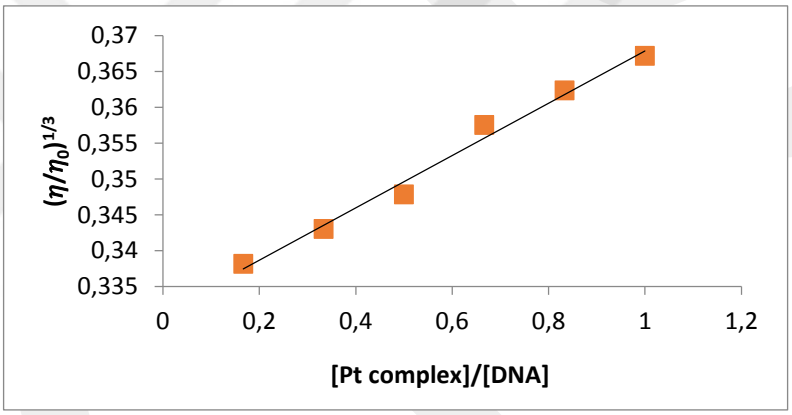

Figure 3.7. The changes in the relative viscosity of the ct-DNA in the presence of $PtLCl_2$.

Groove binding or surface binding nature of $PtLCl_2$ is clearly demonstrated through the increase of the relative viscosity of ct-DNA by $PtLCl_2$ in an extent which is lesser than the similar interaction of EB [25].

3.2.4 Fluorometry

Further information on the localization of the drugs and the interaction mode with DNA can be provided through the fluorescence spectroscopy technique [43]. Quenching of the fluorescence is described by the Stern-Volmer equation below [44]:

$$\frac{I_o}{I} = 1 + K_{sv} \, . r$$

In the above equation, (I_0) represents the fluorescence intensity in the absence of quencher, while (I) is the same parameter in the presence of the quencher and r demonstrates the ratio of concentration of the quencher to the DNA. The fluorescence intensity is enhanced as a result of the interaction of complexes with DNA due to several reasons [45]. An intercalative interaction is exhibited through the increase in fluorescence emission intensity of the DNA-EB system with the increase of the complex concentration [35].

The Stern-Volmer quenching constant (K_{sv}) can be calculated using the ratio of the slope to the intercept of the plot of I_0/I *vs* r for the $PtLCl_2$ in the presence of a quencher. Due to the EB strong intercalation between the base pairs of DNA, the EB produces intense fluorescence in the presence of DNA. In the literature, it is mentioned that the fluorescence is quenched through the addition of a second molecule [46]. In order to determine the extent of binding between $PtLCl_2$ and the DNA, fluorescence quenching is carried out with EB bound DNA while increasing concentration of $PtLCl_2$. There are no changes in emission intensity in the reference experiment of $PtLCl_2$ complex with EB, where EB concentration is kept constant and concentration of $PtLCl_2$ is increased. Nevertheless, the emission intensity decreases when the DNA is added as shown in Figure 3.8 below, which can be attributed to the quenching can caused by the substitution of the EB with $PtLCl_2$. The K_{sv} value calculated for the $PtLCl_2$ complex as 0.0044, which is a low value that confirms the weak intercalative binding modes of the $PtLCl_2$ [35,47,48].

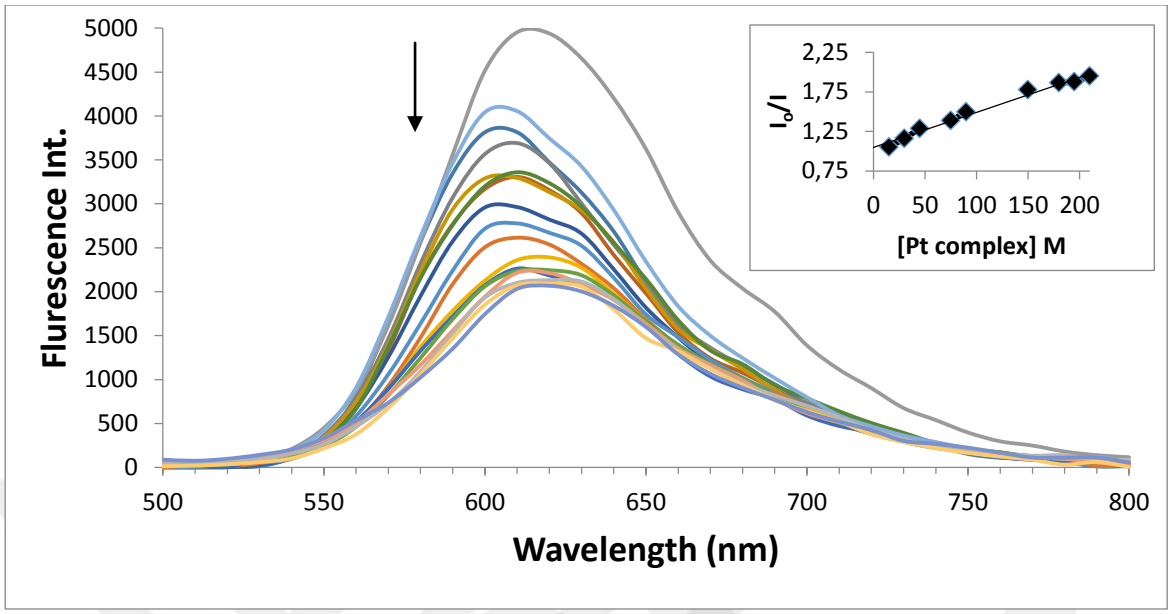

Figure 3.8. Fluorescence spectra observed upon addition of $PtLCl_2$ to the EB bound CT-DNA.

3.3 BSA Interaction

3.3.1 UV-VIS

The electronic absorption titration experiments were performed with a fixed BSA concentration, while increasing the $PtLCl_2$ complex concentration and recording the the change in absorption caused by the tryptophan and tyrosine aromatic amino acids [15] [16]. Furthermore, the BSA to $PtLCl_2$ molar ratio was varied from 1 to 10 and the optimum incubation time is 45 minutes. The hypochromic interaction (Fig.3.9) is attributed to π-π stacking between the aromatic rings of the $PtLCl_2$ and the phenyl rings of the tryptophan, tyrosine and phenylalanine residues of the BSA [49]. By plotting $1/(A-A_o)$ versus $1/[PtLCl_2]$, and getting the ratio between the intercept and the slope, the binding constant (K_b) is calculated as $4.6x10^5$ M^{-1} at 37 ^oC. This result indicates a strong interaction between BSA and $PtLCl_2$ complex as mentioned before with a range of 10^5 to 10^6 M^{-1}) in the literature [49].

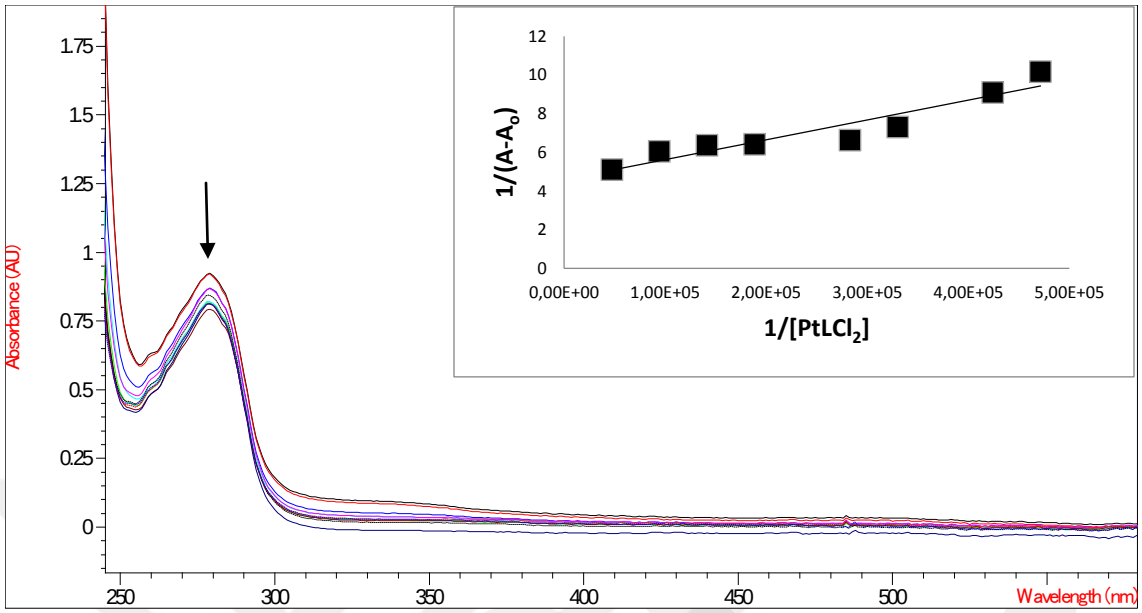

Figure 3.9. Electronic absorption spectra of the BSA in NaPi buffer (pH 7.4) in the absence and presence of increasing amounts of the platinum complex at 37 ^{o}C. Inset: Plot of $1/(A - A_o)$ versus $1/[Pt(L)Cl_2]$.

Moreover, the thermodynamic parameters of the interaction were determined at different temperatures ranging from 37 to 67^{o}C by using Van't Hoff equation as shown in the Figure 3.10 & 3.11 and table 3.5 below [50]:

$$\ln k = \frac{-\Delta H}{RT} + \frac{-\Delta S}{R}$$

$$\Delta G = -RT\ lnK$$

$$\Delta S = \frac{\Delta H - \Delta G}{T}$$

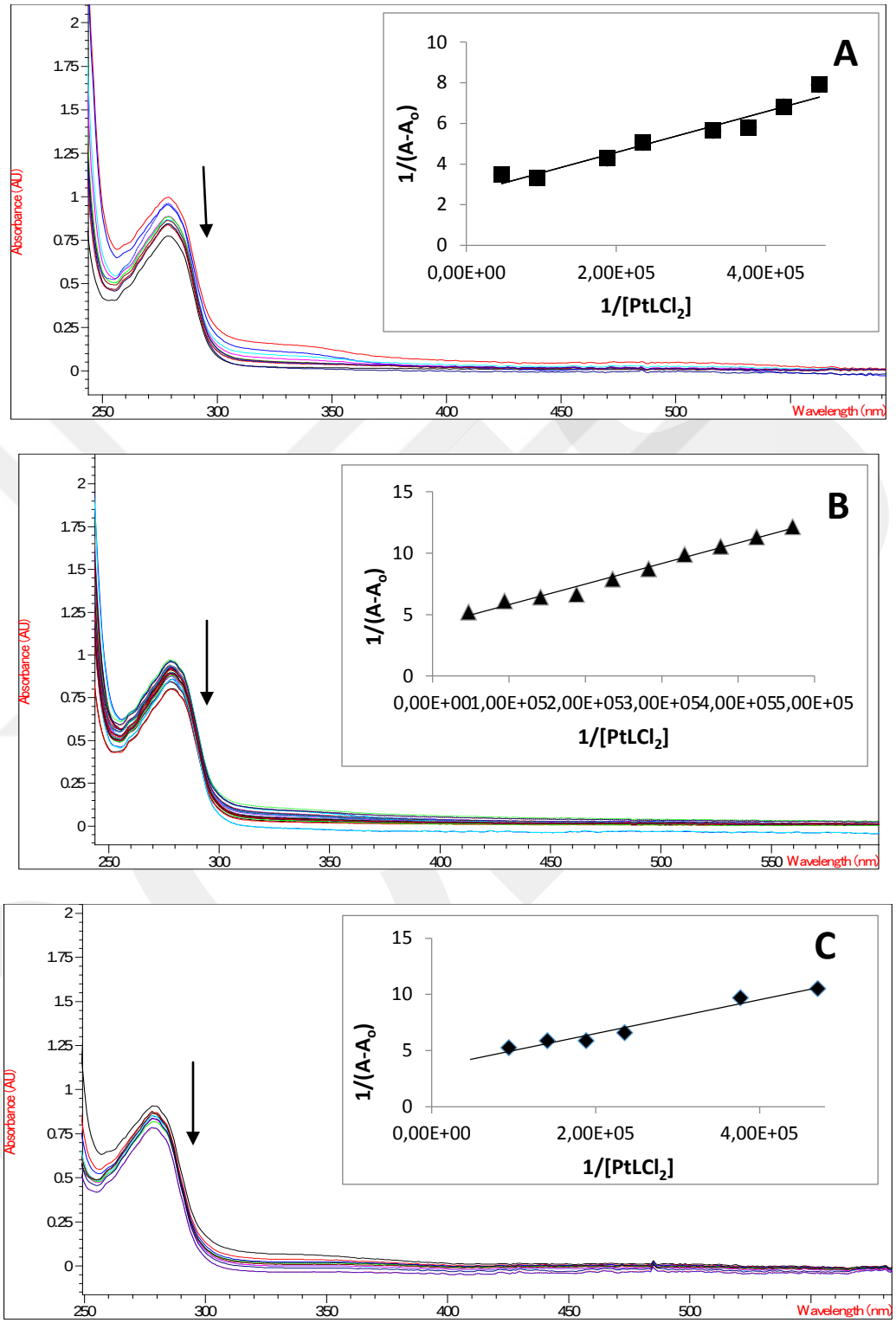

Figure 3.10. Electronic absorption spectra of the BSA at (A) 45 ^{o}C, (B) 57 ^{o}C and (C) 67 ^{o}C, respectively, in NaPi buffer (pH 7.4) in the absence and presence of increasing amounts of the platinum complex. Inset: Plot of $1/(A - A_o)$ versus $1/[Pt(L)Cl_2]$.

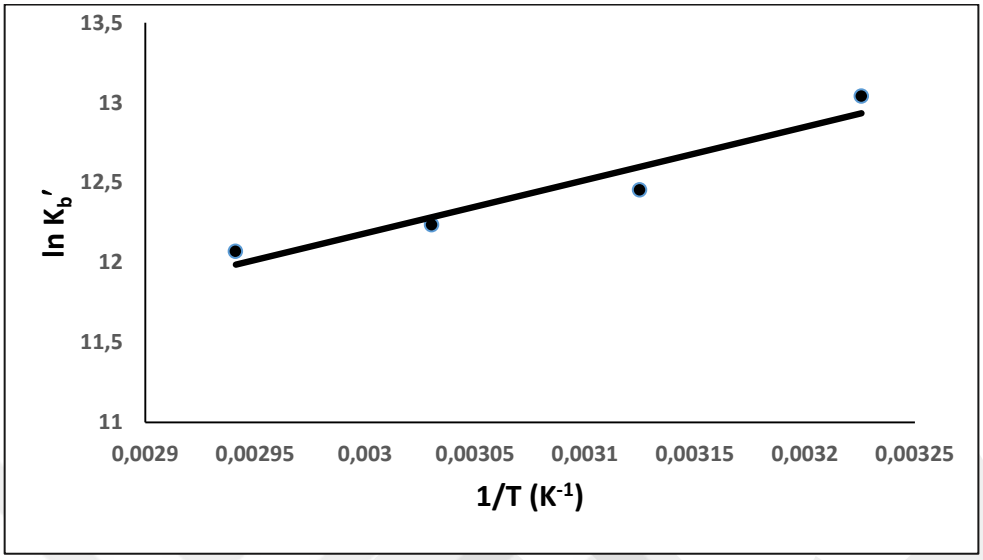

Figure 3.11. The linear Van't Hoff plot based on ln K_b' versus 1/T.

TABLE 3.5. ΔG°, ΔH^o and ΔS^o data for BSA-$PtLCl_2$ adduct

TEMP(K)	K_b' (M^{-1})	ΔG°((kJ mol^{-1})	ΔH°((kJ mol^{-1}))	ΔS°(J/K)
310	4.60 x 10^5	-33.6084	-27.6	18.492
320	2.57 x 10^5	-33.1361		
330	2.06 x 10^5	-33.5746		
340	1.75 x 10^5	-34.1208		

Through the results of the thermodynamic parameters, the low value of the enthalpy changes (ΔH^o), regardless of its sign, along with a positive entropy change (ΔS^o) indicate electrostatic interactions. Furthermore, the negative value of the Gibbs free energy changes (ΔG^o) indicates that the interaction between the BSA and $PtLCl_2$ is spontaneous [50,51].

3.3.2 Thermal Decomposition

Precipitation, crystallization and denaturation of proteins are processes that are illustrated through the utilization of organic solvents [52], which impact the status of solvated ions and challenge interactions of the particles [53]. Furthermore, cations vary from anions through the solvated state, which impose an impact on protein stability [54].

Thermal stability is imposed, which enhances its index, through the binding of the complex to the original status of the protein. Through the carried out experiment, the thermal denaturation of BSA was measured in the case of absence and the case of presence of the $PtLCl_2$ in order to examine the extent of thermal stabilization of BSA when the binding. The thermal denaturation is graphed by obtaining the absorbance changes of the BSA at 280 nm versus temperature. The increase of the transition temperature of BSA when the $PtLCl_2$ is added is an evidence of a partial denaturation of BSA attributed to $PtLCl_2$ due to the partial exposure of various groups to the solvent environment.

The melting temperature of BSA is obtained as 96 ^{o}C in the experiment. Thereafter, the $PtLCl_2$ addition increased the melting point of BSA by 7 ^{o}C to reach to 103 ^{o}C, Figure 3.12. Therefore, the findings of the experiment indicate that BSA becomes more stable upon binding with the $PtLCl_2$ complex.

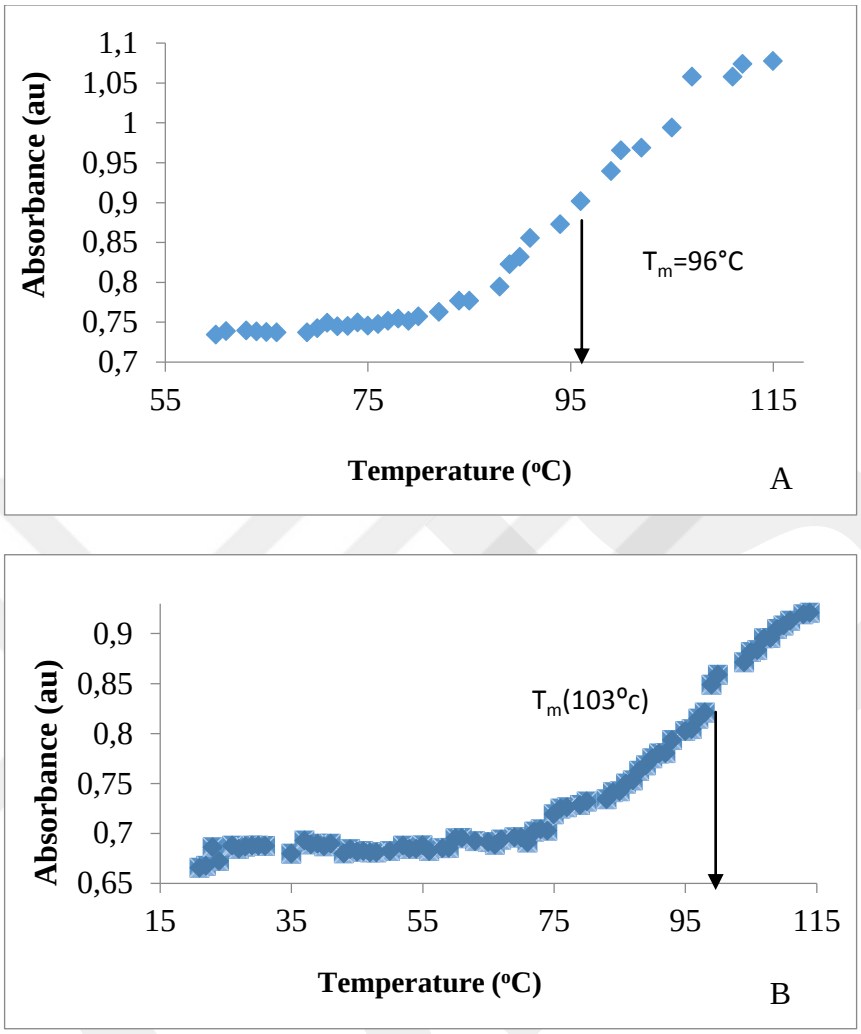

Figure 3.12. Thermal denaturation plot of BSA obtained between 30-115 ^{o}C in 0.5 M NaPi at pH:7.4 (A) without and (B) with the $PtLCl_2$ complex.

3.3.3 Viscosity

The binding mode between $PtLCl_2$ and BSA is further examined through measurements. The viscosity of the solution increases, through literature evidence, due to the electrostatic interaction between metal complexes and BSA [55]. Therefore, when the binding happens in the BSA grooves, there are minor positive or negative changes occur in the protein solution relative viscosity, which can be observed [56]. Nonetheless, a

hydrophobic interaction is exhibited through the increase of the relative viscosity of the protein solution with the increase of the concentration of the metal complex [57].

The binding mode of the platinum complex to BSA was examined through viscometric titration. An incubation process was carried out at 37 ^{o}C during the 45 minutes prior the execution of the experiment. The viscosity measurements were obtained through SV-10 VIBRO viscometer, which shows an increase in the BSA viscosity through the comparison of the results of the standalone $PtLCl_2$.

Figure 3.13 illustrates the increase of concentration $PtLCl_2$ as a ratio to BSA, and its impact on the specific viscosity values $(\eta/\eta_o)^{1/3}$ (η and η_o) in the presence and the absence of $PtLCl_2$. Therefore, the viscosity clearly increases for the solution, indicating an interaction in hydrophobic region of the protein, as the $PtLCl_2$ is added to the BSA solution [58].

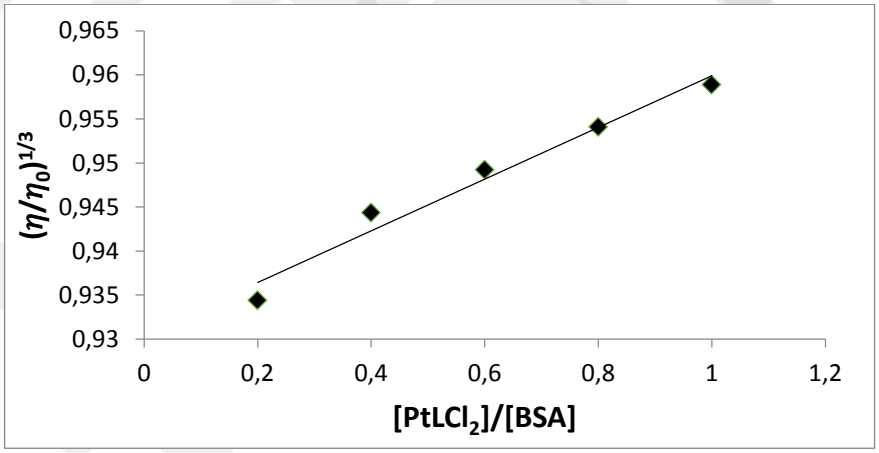

Figure 3.13. The changes in the relative viscosity of BSA in the presence of the $PtLCl_2$ complex.

3.3.4. Fluorometry

Studying the fluorometry of the BSA and $PtLCl_2$ facilitates good identification about the binding type of the complex to BSA. The BSA fluorescence emission is recorded at around 346 nm, which does not change by increasing the concentration of $PtLCl_2$. There are three fluorescent amino acids in BSA, which are tryptophan (which has the most essential part in the quenching), tyrosine and phenylalanine [59]. The process of examining the fluorescence emission intensity of the band at 560 nm in the presence of $PtLCl_2$ while using several sodium phosphate buffer (pH 7.4) concentrations and excitement at 280 nm was carried out. There is a decrease in the emission intensity of the characteristic band of the protein sample at 560 nm with the increase of the concentration of $PtLCl_2$ as shown in Figure 3.14.

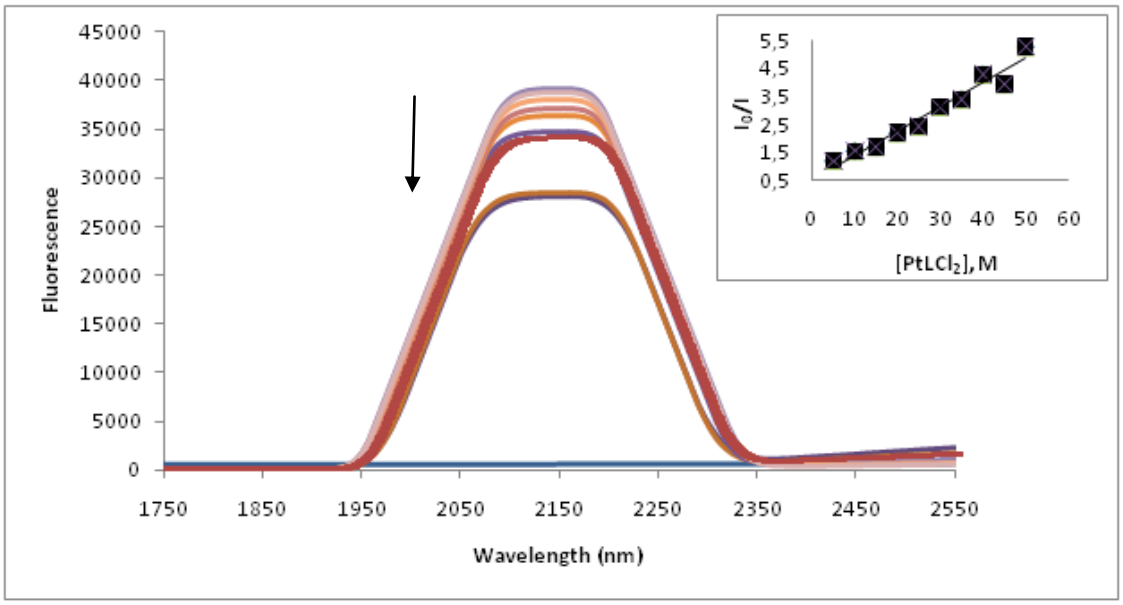

Figure 3.14. The fluorescence spectra observed upon addition of $PtLCl_2$ to the BSA solution.

BSA fluorescence quenching in the presence of $PtLCl_2$ is identified by a linear Stern-Volmer (SV) plot (Fig. 3.14) as denoted as in experimental part:

$$\mathbf{I_o / I = 1 + K_{SV}.r} \qquad \mathbf{(8)}$$

The K_{sv} of the is found to be 0.157, which is much smaller than the reported ones in the literature [59,60]revealing a weak interaction. Since the maximum emission intensity of BSA does not shift or change much with the effect of the platinum complex, it was suggested that $PtLCl_2$ might interact with BSA through the hydrophobic region located inside the protein [61].

The electronic absorption titration was also used to indicate the kind of quenching by the $PtLCl_2$ on the BSA. As shown in Figure 3.14, it is evident that there were no changes to the position of the absorption intensity of the BSA, recorded at 278 nm accompanying an increase of its value. Such a result indicates a static quenching process [60], which is attributed to the complex formation between the molecules of the BSA and $PtLCl_2$ complex [50].

3.4 FTIR

The stability of the interaction between BSA and $PtLCl_2$ is investigated for 14 days by taking spectra of the sample every day. Figure 3.15 shows the spectra of BSA with $PtLCl_2$ at the first day and at the 14^{th} day of incubation. Comparing the two spectra reveals that there are no major time-dependent changes. Although the structure of protein is influenced by the presence of $PtLCl_2$, the changes in the protein structure are instant and remain the same for two weeks. It is also obvious from the figure that DMF has strong absorbance in the IR spectrum.

Table 3.6: FTIR Spectra Assignment			
	Wavelength		**Wavelength**
DMF $\rho C'H_3 + \rho C''H_3$	1062 cm^{-1}	**DMF** $\delta_a C'H_3$	1438 cm^{-1}
DMF $\rho C'H_3 + \nu CN$	1090 cm^{-1}	**BSA + $PtLCl_2$** **C-N-H bending**	1497 cm^{-1}
BSA + Cis7	1108 cm^{-1}	**DMF** **ν(N-C)**	1507 cm^{-1}
DMF $\delta NCH + \delta C''H_3$	1385 cm^{-1}	**BSA or BSA+ $PtLCl_2$** **ν(C-N)**	1540 cm^{-1}
BSA + $PtLCl_2$ δCH_3	1391 cm^{-1}	**BSA + $PtLCl_2$** **ν(C=C)**	1650 cm^{-1}
DMF $\delta_a C'H_3 + \delta_a C''H_3$	1407 cm^{-1}	**BSA** **ν(C=C)**	1655 cm^{-1}
BSA + $PtLCl_2$ **ν(C-C)**	1420 cm^{-1}	**DMF** **ν(C=O)**	1657 cm^{-1}

Characteristic peaks of DMF and sample are identified and the results are summarized in Table 3.6 [62,63,64,65]. The IR spectrum of the pyrazine peak, observed at around 1438 cm^{-1}, is caused by the CH_3 deformation in DMF. The peaks observed in the range 1660-1630 cm^{-1} are assigned to the C=O mode mainly originating from the protein backbone. The peaks appeared in the range of 1000-1300 cm^{-1} are due to $\rho C'H_3 + \rho C''H_3$ and $\rho C'H_3 + \nu CN$ rocking and stretching frequencies.

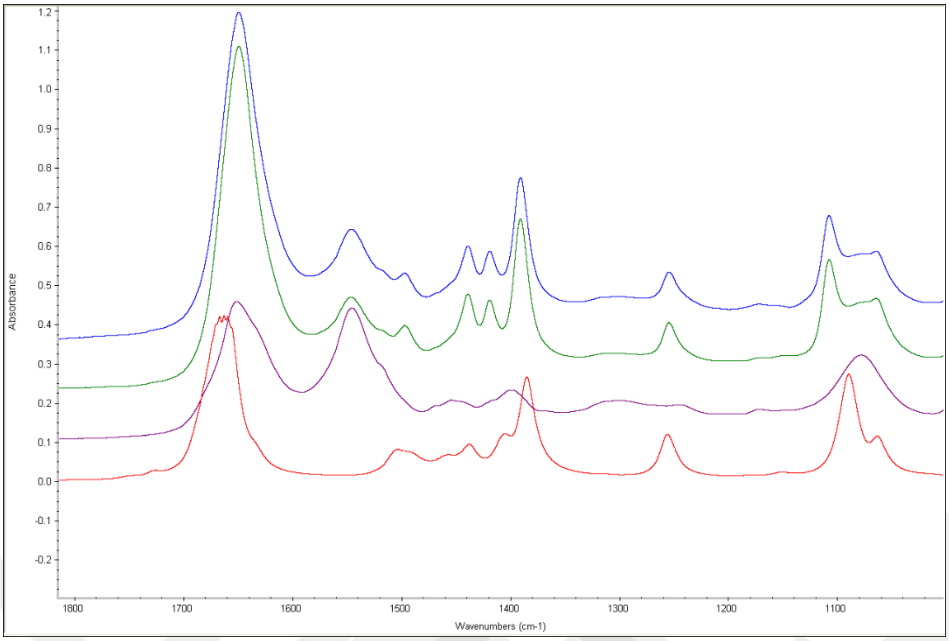

Figure 3.15. IR absorbance spectra of BSA with $PtLCl_2$ at the 1st day (blue trace) and 14th day (green trace) of incubation. The spectrum of BSA blank (purple trace) and DMF blank (red trace) are also given for comparison. Spectra are manually shifted to be equally spaced along the vertical axis for better visual comparison.

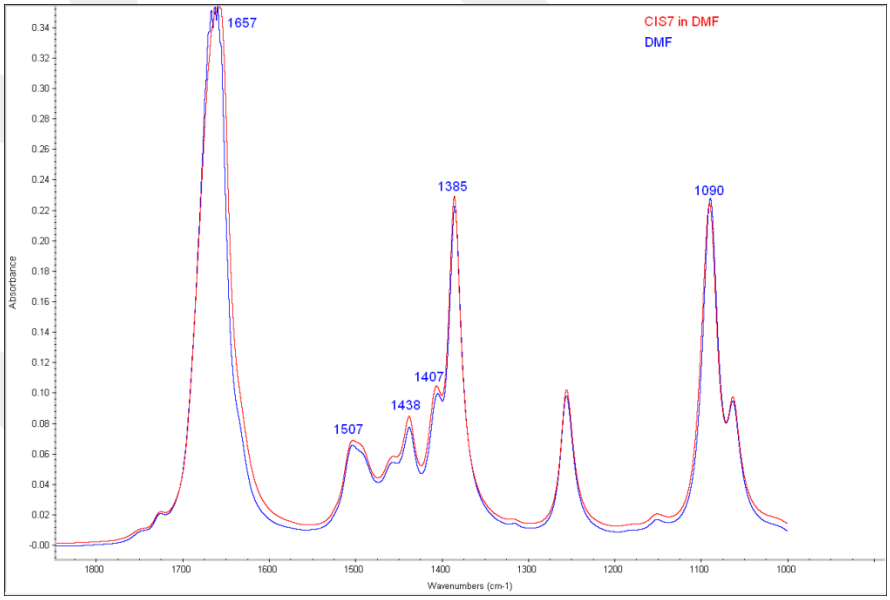

Figure 3.16. The IR spectrum of $PtLCl_2$ dissolved in DMF (red trace) and the spectrum of DMF alone (blue trace).

Strong absorbance of the complex in the fingerprint region is not due to the $PtLCl_2$ absorbance but because of the solvent DMF. Figure 3.16 shows the two respective spectra. They are nearly identical. Therefore, a rise in a band cannot be attributed to the effect of $PtLCl_2$ but band shifts are good indicators of a possible interaction between the protein and the complex. Thus, the second derivative spectra are calculated for the spectra of samples at the first day and at the 14^{th} day of incubation, as well as the spectra of the reference blank samples.

In the first region of the spectrum, the blank BSA has strong absorbance at 1655 cm^{-1} which is due to the alpha-helical content of the protein. DMF also has an absorbance probably due to the C=O stretching mode at 1657 cm^{-1}. However, the band representing the helices shifts down to 1650 cm^{-1} when BSA interacts with $PtLCl_2$. Lower wavenumber position for this band is attributed to helices surrounded by a more hydrophilic environment or in other words, solvent exposed helices [66]. The change in the environment of helices as indicated by data is probably a result of tertiary structure change; i.e. rearrangement of secondary structures with respect to one another. However, such a change should have decreased the thermal stability of the protein, which is contrary to what has been observed in thermal profiling experiments.

Analysis of amide I and II bands upon complex addition do not show additional changes except the one mentioned above. This leads to the conclusion that the complex does not induce major secondary structure changes in protein, which is an advantage for a candidate drug.

Although blank BSA does not have a significant absorbance at ~1420 cm^{-1}, upon interacting with $PtLCl_2$, an intense band appears. This position is attributed to a CH_2 group attached to a carbonyl, nitrile or nitro group [66]. Although the spectral change is drastic, it is not possible to pinpoint the origin of this change since CH_2 is a very common group in all three different samples. Another band that shows a position change is the 1090 cm^{-1} (in DMF) shifting to 1108 cm^{-1} (DMF and BSA). This band is also attributed to CH_2 rocking mode.

CHAPTER 4

CONCLUSIONS

Through this research, a platinum complex containing 5,6-di-(pyridine-2-yl)-2,3-dihydropyrazine ligand was synthesized and analyzed using electronic absorption spectrum, ^{1}H-NMR, FTIR spectroscopy methods.

The DNA binding existence with $PtLCL_2$ complex was examined through spectroscopic methods. Therefore, the binding constant, K_b, of $PtLCL_2$ to DNA was as 6.67×10^3 M^{-1}. A weak action mode through electrostatic mode or groove binding of $PtLCL_2$ to DNA is proven through the UV titration experiment.

The temperature dependent binding constant (K'_b) was determined at 310, 320, 330 and 340 K in order to examine the nature of interaction between $PtLCL_2$ and DNA. Subsequently, the standard Gibbs Free energy change (ΔG^o) was calculated by using these K'_b values. The negative value of ΔG^o revealed the interaction is a spontaneous process. The ΔH^o values of the platinum complex was at around (-24.37 kJ/mol), and the ΔS^o value was at around (-6.094 J/mol K). These changes are an evidence of the entrophy motivated binding, which indicates an intercalative action mode.

Moreover, fluorescence quenching experiment, conducted with the platinum complex with EB in the presence of DNA, show a decrease in the emission intensity. These quenching can be associated with the substitution of the EB with the platinum complex or might be ascribed with the groove binding mode, in which the EB binding areas might be hidden by the complex association through the grooves. The K_{sv} values obtained for the platinum complex in case of the DNA are 0.0044. Low K_{sv} values also confirm the weak intercalative binding modes of the platinum complex.

FTIR results do not show the exact location of the binding site for the complex; however, they clearly show that the helices in the structure of BSA are solvent exposed

upon interacting with $PtLCl_2$. Therefore, it is possible to argue that the complex is targeting the hydrophobic core of the protein, making it more open to solution, at least partially if not mostly. Such a tertiary structure change should have destabilized the protein; however, thermal stability experiments showed a more stable protein structure when in complex with $PtLCl_2$. Furthermore, the incubation tests argue that the interaction between the protein and the complex is instant and does not change in time. Apart from tertiary structure changes, the complex does not induce any detectable secondary structure change in BSA.

REFERENCES

[1] ACS, "Cancer Facts & Figures 2016," American Cancer Society Inc., Atlanta, 2016.

[2] L. Hartwell, "Cell Biology and Cancer," *REDISCOVERING BIOLOGY: Molecular to Global Perspectives,* 2003.

[3] ACS, "Chemotherapy Drugs: How They Work," American Cancer Society Inc., Atlanta, 2015.

[4] S. Van Zutphen, Targeting Platinum Compounds: Synthesis and Biological Evaluation, Leiden: F&N Boekservice/ Eigen Beheer, 2005.

[5] I. Ali, W. A. Wani, K. Saleem and A. Haque, "Platinum Compounds: A Hope for Future Cancer Chemotherapy," *Anti-Cancer Agents in Medicinal Chemistry,* pp. 296-306, 2013.

[6] C. F. J. Barnard, "Platinum Anti-Cancer Agents: Twenty Years of Continuing Development," *Platinum Metals Review,* pp. 162-167, 1989.

[7] S. Gowda KR, B. B. Mathew, C. N. Sudhamani and H. S. B. Naik, "Mechanism of DNA Binding and Cleavage," *Biomedicine and Biotechnology 2 (1),* pp. 1-9, 2014.

[8] CSLS, "Nucleic Acids," 10 April 2012. [Online]. Available: http://csls-text3.c.u-tokyo.ac.jp/active/06_05.html.

[9] N. J. Turro, J. K. Barton and D. A. Tomalia, "Molecular recognition and chemistry in restricted reaction spaces. Photophysics and photoinduced electron transfer on the surfaces of micelles, dendrimers, and DNA," *Accounts of Chemical Research 24(11),* pp. 332-340, 1991.

[10] H. Y. Mei and H. Y. Barton, "Chiral probe for A-form helixes of DNA and RNA: tris(tetramethylphenanthroline)ruthenium(II)," *Journal of the American Chemical*

Society 108 (23), p. 7414–7416, 1986.

[11] T. A. V. D. Berg, "Oxidative cleavage of DNA," in *Iron catalyzed oxidation chemistry: from C-H bond activation to DNA cleavage*, Groningen, University of Groningen, 2008, pp. 2-25.

[12] T. Topala, A. O. L. Bodoki and R. Oprean, "Bovine Serum Albumin Interactions with Metal Complexes," *Clujul Medical,* vol. 87, no. 4, pp. 215-219, 2014.

[13] S. Roy, "Review on Interaction of Serum Albumin with Drug Molecules," *Journal of Pharmacology and Toxicological Studies,* vol. 4, no. 2, pp. 7-16, 2016.

[14] B. X. Huang, H.-Y. Kim and C. Dass, "Probing three-dimensional structure of bovine serum albumin by chemical cross-linking and mass spectrometry," *Journal of the American Society for Mass Spectrometry,* vol. 15, no. 8, p. 1237–1247, 2004.

[15] P. F. Spahr and J. T. Edsall, "Amino Acid Composition of Human and Bovine Serum Mercaptalbumins," *The Journal of Biological Chemistry,* vol. 239, no. 3, pp. 850-854, 1964.

[16] S. Ma, M. Nishikawa, Y. Yabe, F. Yamashita and M. Hashida, "Role of tyrosine and tryptophan in chemically modified serum albumin on its tissue distribution," *Biol Pharm Bull,* vol. 29, no. 9, pp. 1926-1930, 2006.

[17] The Biology Project, "Tyrosine Y (Tyr)," The Biology Project, 25 August 2003. [Online]. Available: http://www.biology.arizona.edu/biochemistry/problem_sets/aa/Tyrosine.html. [Accessed 22 May 2017].

[18] TutorVista, "Tryptophan," TutorVista, 19 July 2012. [Online]. Available: http://chemistry.tutorvista.com/biochemistry/tryptophan.html. [Accessed 21 May 2017].

[19] Y. N. Chirgazde and N. A. Nevskaya, "Infrared spectra and resonance interactions of amide-I and II vibration of alpha-helix," *Biopolymers,* vol. 15, no. 4, pp. 637-

648, 1976.

[20] W. Mantele, "Reaction-induced infrared difference spectroscopy for the study of protein function and reaction mechanisms," *Trends Biochem. Sci.,* vol. 18, pp. 197-202, 1993.

[21] A. Harold, Goodwin and F. Lions, "Tridentate chelate compounds II," *J. Am. Chem. Soc.,* vol. 81, p. 6415, 1959.

[22] A. Wolfe, G. H. Shimer Jr and T. Meehan, "Polycyclic aromatic hydrocarbons physically intercalate into duplex regions of denatured DNA," *Biochemistry (American Chemical Society),* vol. 26, no. 20, pp. 6392-6396, 1987.

[23] H. Wu, X. Huang, J. Yuan, F. Kou, G. Chen, B. Jia, Y. Yang and Y. Lai, "Synthesis, Crystal Structure and DNA-binding Properties of a Nickel(II) Complex with 2, 6-Bis(2-benzimidazolyl)pyridine," *Z. Naturforsch,* vol. 65b, p. 1334 – 1340, 2010.

[24] J. R. Lakowicz and B. Weber, "Quenching of fluorescence by oxygen: Probe for structural fluctuations in Macromolecules," *Biochemistry,* vol. 12, pp. 4161-4170, 1973.

[25] S. M. Afzal and e. al., "Physicochemical and Nonlinear Optical Properties of Novel Environmentally Benign Heterocyclic Azomethine Dyes: Experimental and Theoretical Studies," *PloS one,* vol. 11, no. 9, 2016.

[26] P. A. Ajibade and e. al, "Synthesis and characterization of Ni (II), Pd (II) and Pt (II) complexes of 2, 4-diamino-5-(3, 4, 5-trimethoxybenzyl) pyrimidine complexes," *Journal of Coordination Chemistry,* vol. 59, no. 14, pp. 1621-1628, 2006.

[27] L. Rahman and e. al, "Recent advances in synthesis, characterization and biological activity of nano sized Schiff base amino acid M (II) complexes," *International Journal of Nano Chemistry,* vol. 1, no. 2, pp. 79-95, 2015.

[28] A. L. M. Batista de Carvalho, S. M. Fiuza, J. Tomkinson, L. A. E. Batista de Carvalho and M. P. M. Marques, "Pt(II) Complexes with Linear Diamines—Part I: Vibrational Study of Pt-Diaminopropane," *Spectroscopy: An International Journal*, vol. 27, no. 5-6, pp. 403-413, 2012.

[29] P. R. Reddy and E. al, "Synthesis and DNA cleavage properties of ternary Cu (II) complexes containing histamine and amino acids," *Tetrahedron Letters*, vol. 47, no. 41, pp. 7311-7315, 2006.

[30] P. R. Reddy, K. S. Rao and B. Satyanarayana, "Synthesis and DNA cleavage properties of ternary Cu (II) complexes containing histamine and amino acids," *Tetrahedron Letters*, vol. 47, no. 41, pp. 7311-7315, 2006.

[31] M. J. Waring, "Complex formation between ethidium bromide and nucleic acids," *Journal of molecular biology*, vol. 13, no. 1, pp. 269-282, 1965.

[32] R. B. Nair and e. al, "Synthesis and DNA-Binding Properties of [Ru(NH3)4dppz]2+," *Inorganic Chemistry*, vol. 37, no. 1, pp. 139-141, 1998.

[33] R. R. Pulimamidi and e. al, "Picolinic acid based Cu(II) complexes with heterocyclic bases--crystal structure, DNA binding and cleavage studies," *European Journal Medical Chemistry*, vol. 79, pp. 117-127, 2014.

[34] S. Arounaguiri and B. G. Maiya, "Dipyridophenazine Complexes of Cobalt(III) and Nickel(II): DNA-Binding and Photocleavage Studies," *Inorganic Chemistry*, vol. 35, no. 14, pp. 4267-4270, 1996.

[35] G. Zhang and e. al, "Spectroscopic studies on the interaction of morin–Eu(III) complex with calf thymus DNA," *Journal of Molecular Structure*, vol. 923, no. 1-3, pp. 114-119, 2009.

[36] Arjmand F., Parveen S., Afzal M., Shahid M., Synthesis, characterization, biological studies, “DNA binding, cleavage, antibacterial and topoisomerase I) and molecular docking of copper(II) benzimidazole complexes”. J. Photochem.

Photobiol. B., Biology, **2012**, 114,15-26.

[37] K. P. R. Reddy and A. Shilpa, "Interaction of DNA with small molecules: Role of copper histidyl peptide complexes in DNA binding and hydrolytic cleavage," *Indian journal of chemistry,* vol. 49A, pp. 1003-1015, 2010.

[38] N. Nikolis, C. Methenitis and G. Pneumatikakis, "Studies on the interaction of altromycin B and its platinum (II) and palladium (II) metal complexes with calf thymus DNA and nucleotides," *Journal of inorganic biochemistry,* vol. 95, no. 2, pp. 177-193, 2003.

[39] J. B. Chaires, "Allosteric conversion of Z DNA to an intercalated right-handed conformation by daunomycin," *Journal of Biological Chemistry,* vol. 261, no. 19, pp. 8899-8907, 1986.

[40] J. L. Garcia-Gimenez, G. Alzuet, M. Gonzales-Alvarez, M. Liu-Gonzales, A. Castineiras and J. Borras, "Oxidative nuclease activity of ferromagnetically coupled μ-hydroxo-μ-propionato copper(II) complexes $[Cu_3(L)_2(\mu\text{-}OH)_2(\mu\text{-propionato})_2]$ (L = N-(pyrid-2-ylmethyl)Rsulfonamidato, R = benzene, toluene, naphtalene)," *J. Inorg. Biochem,* vol. 103, pp. 243-255, 2009.

[41] P. Kumar, I. Gorai, M. K. Santra, B. Mondal and D. Manna, "DNA binding, nuclease activity and cytotoxicity studies of Cu(II) complexes of tridentate ligands," *Dalton Trans.,* vol. 41, pp. 7573-7581, 2012.

[42] D. Suh and J. B. Chaires, "Criteria for the mode of binding of DNA binding agents," *Bioorganic & medicinal chemistry,* vol. 3, no. 6, pp. 723-728, 1995.

[43] V. e. a. Gonzalez-Ruiz, An overview of analytical techniques employed to evidence drug-DNA interactions. Applications to the design of genosensors, INTECH, 2011.

[44] J. R. Lakowicz, Principles of Fluorescence Spectroscopy, 3rd Edition, Springer, 2006.

[45] F.-Y. Wu and e. al, "Study of interaction of a fluorescent probe with DNA," *Journal of Luminescence,* vol. 129, no. 11, pp. 1286-1291, 2009.

[46] A. S. Abu-Surrah and M. Kettunen, "Platinum group antitumor chemistry: design and development of new anticancer drugs complementary to cisplatin," *Current medicinal chemistry,* vol. 13, no. 11, pp. 1337-1357, 2006.

[47] M. Muralisankar, S. Sujith, N. S. P. Bhuvanesh and A. Sreekanth, "Synthesis and crystal structure of new monometallic and bimetallic copper (II) complexes with N-substituted insatin thiosemicarbazone ligands: Effects of the complexes on DNA/protein-binding property, DNA cleavage study and in vitro anticancer activity," *Polyhedron,* vol. 118, pp. 103-117, 2016.

[48] F. Ahmadi, N. Ebrahimi-Dishabi, K. Mansouri and F. Salimi, "Molecular aspect on the interaction of ainc-ofloxacin complex with deoxyribonucleic acid, proposed model for binding and cytotoxicity evalaution," *Research in Pharmaceutical Sciences,* vol. 9, no. 5, pp. 367-383, 2014.

[49] M. Hazra, T. Dolai, A. Pandey, S. K. Dey and A. Patra, "Fluorescent copper(II) complexes: The electron transfer mechanism, interaction with bovine serum albumin (BSA) and antibacterial activity," *Journal of Saudi Chemical Society,* vol. 21, pp. S240-S247, 2017.

[50] R. B. Bennie, C. Joel, S. D. Abraham, S. T. David and S. I. Pillai, "Structural, Thermal and BSA binding analysis of L-Tryptophan derived Mn(III)/Fe(III) complexes," *Der Pharmacia Lettre,* vol. 8, no. 5, pp. 260-273, 2016.

[51] G. Mandal, M. Bardhan and T. Ganguly, "Interaction of bovine serum albumin and albumin-gold nanoconjugates with L-aspartic acid. A spectroscopic approach," *Colloids and Surfaces B: Biointerfaces,* vol. 81, pp. 178-184, 2010.

[52] T. Arakawa, Y. Kita and S. N. Timasheff, " Protein Precipitation and Denaturation by Dimethyl Sulfoxide," *Biophys. Chem,* vol. 131, no. 1–3, p. 62–70, 2007.

[53] H. A. Shilajyan, "Electrical Conductivity of Potassium Salt–Dimethylsulfoxde–Water Systems at Different Temperature," *Proceedings of the YSU. Biology and Chemistr*, no. 1, p. 3–6, 2013.

[54] K. R. Grigoryan and A. A. Shiladzhyan, "The Effect of Solvated Ions on the Thermal Denaturation of Human Serum Albumin in Water–Dimethylsulfoxide Solutions," *Russian J. of Bioorganic Chemistry*, vol. 35, no. 5, p. 646–649, 2009.

[55] T. Yotsuyanagi, N. Ohta, T. Futo, D. Chen and K. Ikeda, "Multiple and irreversible binding of cis-diamminedichloroplatinum(II) to human serum albumin and its effect on warfarin binding," *Chem. Pharm. Bull.* , vol. 39, pp. 3003-3006, 1991.

[56] U. Kragh-Hansen, "Molecular aspects of ligand binding to serum albumin," *Pharmacol. Rev.*, vol. 33, pp. 17-53, 1981.

[57] L. S. Lerman, "Structural considerations in the interaction of DNA and acridines," *J Mol Biol*, vol. 3, pp. 18-30, 1961.

[58] B. Gowda, M. Mallappa, I. Jayant and R. Rengasamy, "Interaction of Ketoconazole with Bovine Serum Albumin: Electrochemical, Spectroscopic and Molecular Modeling Studies," *J App Pharm Sci*, vol. 5, no. Suppl 2, pp. 37-44, 2015.

[59] R. B. Bennie, S. T. David, C. Joel, S. D. Abraham, M. Seethalakshmi and S. I. Pillai, "Studies on binding affinities of phenylalanine based Schiff base metal complexes on bovine serum albumin," *Der Pharma Chemica*, vol. 6, no. 5, pp. 343-352, 2014.

[60] B. Annaraj, C. Balakrishnan and M. A. Neelakantan, "Synthesis, structure information, DNA/BSA binding affinity and in vitro cytotoxic studies of mixed ligand copper(II) complexes containing a phenylalanine derivative and diimine co-ligands," *Journal of Photochemistry & Photobiology, B: Biology*, vol. 160, pp. 278-291, 2016.

[61] E. Froehlich, J. S. Mandeville, C. J. Jenninge, R. Sedaghat-Herati and H. A. Tajmir-Riahi, *J. Phys. Chem. B* , vol. 113, pp. 6986-6993, 2009.

[62] M. J. Baker, J. Trevisan, P. Bassan, R. Bhargava, H. J. Butler, D. K. M and P. R. Fielden, "Using Fourier transform IR spectroscopy to analyze biological materials," *nature protocols*, vol. 9, no. 8, pp. 1771-1791, 2014.

[63] H. Fabian and W. Mantele, "Infrared Spectroscopy of Proteins (in Biochemical Applications)," John Wiley & Sons Ltd, Chichester , 2002.

[64] K. V. Abrosimova, O. V. Shulenina and P. S. V, "FTIR study of secondary structure of bovine serum albumin and ovalbumin," *Journal of Physics: Conference Series*, vol. 769, no. 1, pp. 1-6, 2016.

[65] F. Korkmaz, D. A. Erdogan and S. Ozalp-Yaman, "Interaction of a novel platinum drug with bovine serum albumin: FTIR and UV-Vis spectroscopy analysis," *new J. Chem*, vol. 39, pp. 5676-5685, 2015.

[66] N. B. Colthup, L. H. Daly and S. E. Wiberley, Introduction to infrared and raman Spectroscopy, 3rd edition, New York: Academic Press, 1990.